VEGF counteracts shear stress-determined arterial fate specification during capillary remodeling.

Dongying Chen[1,*], Oleksii S. Rukhlenko[2], Divyesh Joshi[1], Martina Rudnicki[7], Brian G. Coon[1,#], Raja Chakraborty[1], Anna Tuliakova[2], Elena Ioannou[7], Kathleen A. Martin[1], Christiana Ruhrberg[7], Boris N. Kholodenko[2,3,4,], Martin A. Schwartz[1,5,6,*], Michael Simons[1,5,*]

[1] Yale Cardiovascular Research Center, Department of Internal Medicine, Yale University School of Medicine, New Haven, United States.
[2] Systems Biology Ireland, School of Medicine, University College Dublin, Dublin, Ireland.
[3] Conway Institute of Biomolecular & Biomedical Research, University College Dublin, Dublin, Ireland
[4] Department of Pharmacology, Yale University School of Medicine, New Haven, United States.
[5] Department of Cell Biology, Yale University School of Medicine, New Haven, CT, United States.
[6] Department of Biomedical Engineering, Yale University, New Haven, CT, United States.
[7] UCL Institute of Ophthalmology, London, UK
[#] Current address: Cardiovascular Biology Research Program, Oklahoma Medical Research Foundation, Oklahoma City, United States

* Corresponding authors:
Dongying Chen: dongying.chen@yale.edu
Martin A. Schwartz: martin.schwartz@yale.edu
Michael Simons: michael.simons@yale.edu

Abstract

A key feature of arteriogenesis is capillary-to-arterial endothelial cell fate transition. Although studies over the past two decades reported that vascular endothelial growth factor A (VEGF-A) - VEGFR2 signaling activates Notch to drive this process, how arteriogenesis is regulated remains poorly understood. Here we report that arterial specification is determined by fluid shear stress (FSS) independent of VEGFR2 signaling and that, in contrast to the current paradigm, VEGFR2 signaling must decline for arteriogenesis to fully take place. VEGF-A does not induce arterial fate in capillary endothelial cells, instead, serving as a critical physiological brake to counteract FSS-driven capillary-to-arterial cell fate transition to maintain the capillary state. The transcription factor Sox17 is the key mediator of the FSS-induced arterial program and a target of VEGF-FSS competition. These findings establish a new paradigm of VEGF-FSS crosstalk coordinating angiogenesis, arteriogenesis and capillary maintenance.

Arteriogenesis is defined as the formation of new arteries in response to increasing demand for tissue oxygenation and is initiated when capillary endothelial cells acquire an arterial fate. Despite its importance, the molecular mechanisms regulating this process remain poorly understood[1].

Over the past two decades, a wealth of studies led to a widely accepted principle that highlights VEGF-A (hereafter VEGF) and Notch as drivers of arterial fate specification. This view is based on data showing that VEGF induces Dll4[2-4], which in turn activates Notch[5-7], and that Notch is essential for arterial specification[8-10]. In the mouse retina, gain-of-function (GOF) constitutive Notch activation by overexpression of Notch intracellular domain (NICD) leads to increased and ectopic arterialization[11], while Notch loss-of-function (LOF), achieved by endothelial deletion of Dll4 or treatment with the gamma secretase inhibitor DAPT, results in a hypersprouting phenotype and defective arterial formation[5,12-14]. Therefore, it is reasonable to infer that VEGF, as a Notch inducer, drives arterial specification. Moreover, a recent study proposed that a subset of endothelial cells (ECs) with high VEGF-Notch signaling at the vascular front are selectively committed to an arterial fate as “pre-arterial” ECs[13,15].

Blood flow-induced fluid shear stress (FSS) has also been shown to induce Notch and arterial specification[16-18]. Notably, FSS-induced G1/S cell cycle arrest has been reported as a pre-requisite for arterial fate acquisition[16]. This raises a question of how to reconcile VEGF’s role as a mitogen that drives endothelial proliferation with the need for cell cycle arrest? Although extremely high doses of VEGF or activation of constitutive VEGFR2 signaling have been shown to induce cell cycle arrest[7,19], these conditions are non-physiological and do not provide a definitive answer to address the role of VEGF in arterial specification. Moreover, if physiologically high VEGF signaling is the principal driver of arterial specification, one would expect to find arterialization at the vascular front in the developing retinal vasculature where VEGF levels are the highest and not towards the center of the retina where VEGF levels are relatively low.

To address these critical issues, we set out to analyze arterial specification using the mouse retina as a model. We report here that arterial specification is driven by the FSS independently of VEGF/VEGFR2 signaling and that capillary-to-artery endothelial cell fate transition requires a reduction in VEGF signaling. Furthermore, VEGF signaling serves as a critical physiological brake to counteract FSS-driven arterial fate acquisition by capillary endothelium. Mechanistically, VEGF counteracts the FSS-activated arterial program by reducing Sox17 enrichment on arterial promoters and enhancers. Based on these findings, we propose a novel paradigm by which VEGF-FSS competition coordinates angiogenesis, arteriogenesis and capillary maintenance, thereby resolving long-standing conundrums in arterial specification.

Results

Arteriogenesis occurs in the portion of the capillary bed where VEGF signaling is low.

Vascular morphogenesis in the mouse postnatal retina begins at a postnatal day 0(P0)-1 when nascent vessels begin to sprout from the central vein[20,21] with a rudimentary capillary plexus emerging by P1-2 (Supplemental Fig.1a). At P2-3, when a capillary bed has formed, arterial blood vessels, identified by high-level expression of the arterial marker Sox17 (Sox17^{high}), appear in the central part of the capillary plexus (Supplemental Fig.1a). At P3-4, while sprouting activity continues at the angiogenic front, arteriovenous patterning transforms the central portion of the capillary bed into a hierarchical vascular structure with capillaries, arteries and veins (Supplemental Fig.1a). By P4-5, the whole vasculature has developed into a stereotypical vascular tree: the arteries and the veins alternatively aligned at the central area, the angiogenic sprouts at the periphery driving vascular expansion towards the avascular zone, and the capillary bed in the middle. (Supplemental Fig.1a).

In this developing vasculature, the endothelial phospho-ERK (pERK) signal and EdU-incorporation identified endothelial cells with high level of VEGF signaling, predominantly at the angiogenic front (Supplemental Fig. 1b). Both endothelial pERK levels and EdU-labeled endothelial proliferation activity declined in the capillary bed undergoing arterialization and almost completely disappeared in arterioles and arteries (Supplemental Fig.1b), consistent with previous reports[19]. Systemic intravenous injection of VEGF activated pERK signal in the whole vasculature, including the central portion of capillary bed and in arteries, where pERK signaling was absent in controls (Supplemental Fig.1b). This demonstrates that arterial morphogenesis takes place in the portion of the capillary bed where the VEGF signaling is low.

Blocking VEGFR2 signaling increases arterialization.

To assess the role of VEGF signaling in arterial fate specification during capillary remodeling in the mouse retina, we used a comprehensive set of animal experiments to examine the effect of altering VEGF signaling on angiogenesis and arteriogenesis. Arterial extension was defined as the percentage of the Sox17^{high}- or SMA-labeled blood vessel (arteries) relative to the maximal radial outgrowth from the center of the retina to the periphery labeled by isolectin B4 (IB4). We also quantified the percentage of the un-arterialized gap, defined as the distance between the maximal extent of the Sox17^{high}-labeled arterial tip and the peripheral vascular front, relative to radial outgrowth.

First, we evaluated the effect of inducible global deletion of VEGF-A, the principal activator of VEGFR2. As VEGF is mostly produced in the neural bed[22], we induced global deletion of VEGF-A using Cag-CreER^{TM} (hereafter, *Vegfa*^{iKO}). As expected, deletion of VEGF-A at P2-4 led to significantly reduction in vascular density and the extent of radial outgrowth (Fig.1a). Nevertheless, immunostaining with anti-Sox17 and -SMA antibodies revealed the presence of arteries displaying high level of Sox17 expression (Sox17^{high}), and mural coverage with smooth muscle, in both control and *Vegfa*^{iKO} retinas (Fig.1a). Sox17^{high}-labeled arterial extension in the control retina was 80.3%±4.8% (mean±SD) with a 19.7%±4.4% un-arterialized gap (Fig.1a), while in the *Vegfa*^{iKO} retinas, Sox17^{high}-labeled arterial extension was significantly increased (95.1%±5.1%), with ectopic arterialization in the vascular front and dramatically reduced un-arterialized gap (4.9%±5.1%) (Fig.1a). Moreover, 83.3%±14.2% of all individual arteries measured in the *Vegfa*^{iKO} retinas reached 100% extension (no unarterialized gap), a phenotype not found in the control retinas (Fig.1a). The SMA-labeled arterial extension was reduced in the *Vegfa*^{iKO} retinas (47.3%±22.8%), compared to 59.5%±9.5% in the control retinas (Fig.1a).

To verify these findings, we tested the effect of endothelial VEGFR2 deletion at various time windows before the onset of arteriogenesis (between P2-3), by giving the first dosage of tamoxifen at P0, P1 or early P2, respectively. As expected, tamoxifen induction at P0-2 completely compromised vascular growth at P5, leaving only a tiny vessel at the center of the retina at P5 (Supplemental Fig.2a). Induction at P1-3 resulted in formation of vascular loops at P5, with remarkable reduction in radial outgrowth, vascular density and almost no sprouts (Supplemental Fig.2b), consistent with previous reports[13,14]. Yet Sox17^{high} and SMA staining revealed somewhat variable arterial specification in these *Vegfr2*^{iECKO} vascular loops (Supplemental Fig.2b). In some *Vegfr2*^{iECKO} retinas, the arterial extent was 100%, spanning from the retinal center to the vascular front (Supplemental Fig.2b). Of note, ectopic SMA staining was commonly present at the vascular front and in morphologically venous-like vessels, disrupting the normally alternating arteriovenous alignment (Supplemental Fig.2b). Some *Vegfr2*^{iECKO} retinas had very few blood vessels, in which only trace amount of Sox17^{high} and SMA signal was detected (Supplemental Fig.2b).

Following induction of VEGFR2 deletion at P2-4 (Fig.1b), Sox17^{high}-labeled arterial extension in the *VEGFR2*^{iECKO} retinas was slightly but not significantly higher than the control (84.2%±10.7% vs 79.2%±3.3%) (Fig.1b). Notably, individual measurements per artery revealed that 28.6% of the Sox17^{high}-labeled arteries reached 100% full extension in the *VEGFR2*^{iECKO} retinas, a phenotype of

130 increased arterial specification not found in control animals (Fig.1b). SMA signal in the *VEGFR2*^{iECKO}
131 retinas exhibited high variability and was non-significantly reduced compared to controls (48.1%±14.6%
132 vs 58.1%±3.6%) (Fig.1b).
133 The effectiveness of VEGFR2 deletion in *VEGFR2*^{iECKO} retinas was evaluated by immunostaining
134 with anti-VEGFR2 antibody. In the control retina, VEGR2 signal was present in blood vessels as well as
135 in the neural bed (Supplemental Fig.2c), consistent with a previous report[22]. Intriguingly, in the
136 *VEGFR2*^{iECKO} retina, VEGFR2 staining was absent in the blood vessel but remained in the neural bed,
137 creating an appearance of "empty grooves" in a VEGFR2+ background (Supplemental Fig.2c). These
138 results confirm nearly complete and specific deletion of endothelial VEGFR2 in the *VEGFR2*^{iECKO} retina.
139 Notably, we detected VEGFR2^{null}/Sox17^{high} ECs in the artery-like vessels (Supplemental Fig.2c), a
140 direct evidence of arterial fate specification independent of VEGFR2.
141 Since VEGFR2 deletion could affect more than just VEGFR2 signaling, we studied arteriogenesis in
142 mice with inducible endothelial-specific deletion of PLCγ1 (hereafter *Plcg1*^{iECKO}), the major effector of
143 VEGFR2 signaling[23,24]. Induction of PLCγ1 deletion at P1-3 resulted in compromised angiogenesis at
144 P6 (Fig.1c), in line with the observations in *Vegfa*^{iKO} and *Vegfr2*^{iECKO} retinas. At the same time,
145 arteriogenesis (Sox17^{high} and SMA labeling) was significantly increased (Fig.1c). Quantification
146 revealed that 52.7% of Sox17-labeled and 12.7% SMA-labeled arteries reached 100% extension
147 spanning from the retinal center to the vascular front, which was not found in the control retinas (Fig.1b).
148 Moreover, ectopic arterialization with both Sox17^{high} and SMA signal at the vascular front was
149 evidenced in the *Plcg1*^{iECKO} retinas (Fig.1b).
150 Due to the lack of workable staining antibody, the deletion of endothelial PLC*γ*1 in P6 pups were
151 examined using isolated brain ECs in order to acquire sufficient number of cells for QPCR analysis. The
152 results demonstrate 70% reduction of *plcg1* mRNA as detected by the primers targeting exons2-3 and
153 comparable levels of *plcg1* mRNA by the primers targeting exons 24-26, which confirms effective gene
154 deletion of plcg1 despite the presence of a truncated plcg1 mRNA (Supplemental Fig.3a-b).
155 Lastly, we evaluated the effect of blocking the binding of VEGF and VEGFR2 using DC101, a well-
156 studied neutralizing antibody that specifically blocks the binding of the cognate ligand VEGF-A_{165} to its
157 receptor VEGFR2[25,26], leaving both VEGF-A and VEGFR2 intact and available for other biological
158 activities. DC101 was injected intra-peritoneally into neonatal mice at P1 and P3 and the retinas were
159 evaluated as described above. In agreement with the data from the three other models, DC101
160 treatment inhibited angiogenesis, indicating effective blockade of VEGFR2 signaling (Fig.1d). However,
161 despite a significant reduction in the growth area, vascular density and radial outgrowth, the angiogenic
162 defects caused by DC101 were modest compared to the severe vascular rarefaction phenotypes in the
163 above 3 models, resulting in the preservation of a substantial amount of the vascular bed (Fig.1d).
164 Immunostaining with Sox17 and SMA revealed a very extensive arterialization in the capillary bed, with
165 all arteries labeled by both Sox17^{high} and SMA spanning from the retinal center to the vascular front
166 (100% arterial extension), complete disappearance of the un-arterialized gap, and extensive ectopic
167 arterialization in the capillary bed and veins (Fig.1d).
168 Notch signaling, although not specific to the endothelium, is thought to be an important feature of
169 arterial specification. In order to visualize the effect of blocking VEGFR2 signaling on arterial Notch
170 activity, we crossed the Notch reporter line CBF:H2B-Venus[27] with the *Vegfr2*^{iECKO} and *Plcg1*^{iECKO} mice,
171 respectively. In the control retinas, Notch activity was present in arterial ECs but undetectable in the
172 veins (Supplemental Fig.4). In the *Vegfr2*^{iECKO} and *Plcg1*^{iECKO} retinas, Notch reporter signal (CBF) was
173 clearly detected in the Sox17^{high} arterial ECs (Supplemental Fig.4), suggesting that arterial Notch
174 activity is independent of VEGFR2 signaling.

In summary, data from these four independent approaches showed that VEGFR2 signaling is not required for arteriogenesis. Furthermore, blockade of VEGFR2 signaling compromises angiogenesis but promotes arterial specification in a developing capillary bed.

Fluid shear stress (FSS)-induced arterial specification is independent of VEGFR2 signaling.

Since the arterial program remains intact in *Vegfa*^{iKO}, *Vegfr2*^{iECKO}, *Plcg1*^{iECKO}, and DC101-treated mice, we set out to find the driver of arterial fate specification in these settings. FSS is reported to induce arterial specification[16], which requires the presence of blood flow and, hence, vascular lumenization. To address this question, we retro-orbitally injected Alexa488-conjugated isolectin B4 (IB4-488), which stains only the endothelium in patent vessels with blood circulation. After retinal dissection, retinal whole-mounts were counterstained with Alexa647-conjugated IB4 (IB-647), which stains the whole vasculature, including the patent and the closed vessels. In normal (control) retinas, while the majority of vessels was double-stained, the absence of IB4-488 identified the un-lumenized sprouts at the vascular front and some regressed vessels around the arteries (Fig.2a), indicating a lack of blood flow in these vessels. Importantly, the DC101-treated, *Vegfr2*^{iECKO} and the *Plcg1*^{iECKO} vessels were also well double-stained (Fig.2a), suggesting that there was effective blood flow through these vessels and that the ECs with defective VEGFR2 signaling were exposed to the hemodynamic force (FSS) as a potential driver for arterial specification.

With these data in hand, we next tested whether blocking VEGFR2 signaling affects FSS-induced arterial specification in HUVECs in vitro. HUVECs treated with siPLCγ1 were able to respond to arterial level of laminar FSS (12 dynes/cm^2) with effective induction of a panel of arterial genes, including Sox17, Efnb2, Gja4, Gja5 and Notch target Hey1(Fig.2b). These in vitro findings indicate that FSS-induced arterial specification is independent of VEGFR2 signaling, consistent with the arterial phenotypes of the *Plcg1*^{iECKO} retinas in vivo (Fig.1).

Blocking VEGFR2 signaling promotes capillary-to-artery transition.

To gain mechanistic insights into the arterial phenotypes, we performed single-cell RNAseq analysis of endothelial cells from control and *Plcg1*^{iECKO} mice retinas. Among 30 cell clusters identified in UMAP (uniform manifold approximation and projection) plots, 1505 cells in cluster 12 with endothelial identity (*Pecam1*+, *Cdh5*+; *Cldn5*+) were selected for further analysis (Supplemental Fig.5 and Supplemental Fig.6a). Published markers of endothelial phenotypes (Supplemental Table 1) were used to annotate endothelial zonation in the arterial-capillary-venous axis and determine cell cycle status based on gene expression profiles (Supplemental Fig.6b-f). The following 10 EC subclusters were identified (0-9) (Fig.3a): a sprouting cluster (cluster 6, *Esm1*^{high};*Kcne3*^{high}), an arterial cluster (cluster 9, *Gja4* ^{high};*Gja5*^{high};*Efnb2*^{high};*Sema3g*^{high};*Gkn3*^{high};*Bmx*^{high};*Sox17*^{high};*Cxcl12*^{high};*Unc5b*^{high}, most cells in G1 phase), capillary/venous clusters (clusters 0, 2, 3, 4 and 7, *Aplnr*^{high}; *Mfsd2a*^{high};*Ivns1abp*^{high};*Flt4*^{high};*Tfrc* ^{high};*slc38a5* ^{high};*Nr2f2* ^{high};*Nrp2* ^{high};*Ephb4* ^{high}), an arterial predecessor cluster (cluster 8, with both arterial and capillary profiles) and a proliferative cluster (cluster 0, with capillary/venous profile, all cells in G2M/S phases) (Supplemental Fig.6b-f). In addition, the ECs in cluster 5 display weak endothelial identity with low expression of endothelial markers (Cdh5, Cldn5, Pecam1, Flt1, Kdr and Erg), likely ECs from regressing vessels (Supplemental Fig.6e). The identity of Cluster 1 is unclear, as these ECs express low levels of capillary/venous markers and some endothelial markers (Cdh5, Cldn5 and Kdr) (Supplemental Fig.6d-e).

Analysis of the percentages of ECs in clusters 0-9 revealed substantial reduction in proliferative cluster 0 and capillary clusters 2, 3, 7 in *Plcg1*^{iECKO} ECs (Fig.3b). Notably, in *Plcg1*^{iECKO} ECs, the percentage of arterial predecessors in cluster 8 was substantially increased, while the percentage of arterial ECs in cluster 9 was comparable to that in control (Fig.3b). These findings are consistent with

222 the phenotypes of defective angiogenesis, depletion of the capillary bed and increased arterial
223 specification in the *Plcg1*^{iECKO} retinas (Fig.1b).
224 To understand the developmental transition between these EC clusters, we performed trajectory
225 analyses. Pseudo-time analysis by TSCAN reveals a trajectory starting from proliferative cluster 0 to
226 capillary/venous clusters 4 and 7 and ending at arterial predecessor cluster 8 and arterial cluster 9
227 (Fig.3c). Besides the main C-to-A axis trajectory described above, proliferative cluster 0 also
228 transitioned to cluster 5 with weak EC identity, likely a process of vascular regression (Fig.3c).
229 Meanwhile, capillary/venous cluster 4 and 7 showed side trajectories to sprouting cluster 8 and other
230 capillary/venous clusters 3, 2, 1, respectively (Fig.3c). Finally, RNA velocity analysis confirmed the
231 trajectory of the C-to-A axis in both Control and *Plcg1*^{iECKO} ECs (Fig.3d), which suggests that increased
232 percentage of the *Plcg1*^{iECKO} arterial predecessors in cluster 8 (Fig.3b) is a result of increased C-to-A
233 transition.
234
235 **VEGF counteracts FSS-induced capillary-to-artery endothelial cell fate transition.**
236 The data presented above suggests that VEGF functions as an inhibitor of arteriogenesis by
237 counteracting the FSS-driven arterial specification. To further explore this hypothesis, we used human
238 microvascular blood endothelial cells (HMVBECs) to examine FSS-driven induction of arterial genes
239 and the effect of VEGF on this process. We first carried out RNAseq to study HMVBEC transcriptomic
240 profiles under four different conditions: static (ST), ST+VEGF, FSS, FSS+VEGF (Fig.4a-c). A principal
241 component analysis (PCA) of the transcriptomic responses suggests that ECs assume different cell
242 states under these conditions (Fig.4a). To better understand cell state transitions based on
243 transcriptomics patterns, we applied a systems biology approach termed cell State Transition
244 Assessment and Regulation (cSTAR) analysis[28-30] (Fig.4b, detailed description in legend). Overall, the
245 results of this analysis indicate that the 4 conditions (ST, VEGF, FSS, FSS+VEGF) resulted in four
246 different metastable EC states. The condition of FSS+VEGF led to a new EC state distinct from the
247 FSS state or the VEGF state, which is not a reversion process that VEGF brings the FSS state to the
248 baseline state (ST). This suggests that there are distinct programs activated by both VEGF and FSS
249 with little overlap between the two.
250 These results prompted us to hypothesize that the cell fate transition from capillary (C) state
251 (exposed to both VEGF and FSS) to arterial (A) state (exposed to FSS and declined VEGF) is
252 regulated by FSS-VEGF crosstalk, during which FSS promotes C-to-A transition and VEGF counteracts
253 this process to maintain the capillary fate. Indeed, this idea is supported by transcriptomic profiling of
254 arterial and capillary genes and validation assays (Fig.4c-e). Notably, differential gene expression
255 analysis clustered arterial and capillary gene profiles separately, which are overall inversely regulated
256 by VEGF and FSS (Fig.4c). FSS effectively induced the arterial profile (validated arterial genes Gja4,
257 Gja5, Sox17, Efnb2, Sema3g, Cxcl12, Nrp1, Jag1) and inhibited the capillary profile (validated capillary
258 genes Emcn, Flt4, Mfsd2a; validation RT-PCR of Tfrc and Ivns1abp did not show statistic significant
259 results) (Fig.4c-e). By contrast, VEGF did not induce arterial profile (Fig.4c-e). Instead, when present in
260 the FSS system, VEGF suppressed the FSS-induced arterial profile and rescued the FSS-inhibited
261 capillary profile (Fig.4c-e). While these experiments were conducted using HMVBECs (capillary ECs),
262 our study using HUVECs found a similar expression pattern of arterial genes in response to FSS or
263 FSS+VEGF (Supplemental Fig.7). The only exceptions in HUVECs were the FSS inductions of Sox17
264 and Nrp1, which were upregulated in FSS+VEGF (Supplemental Fig.7), likely due to the venous and
265 embryonic nature of HUVECs. Finally, Immunostaining of arterial markers Sox17 (or SMA) and capillary
266 genes Mfsd2a, Tfrc, Flt4 and Emcn confirmed the inverse pattern of capillary and arterial genes
267 expression in the developing retinal vasculature in mouse neonates (Fig.4f). These results indicate that

268 the FSS promotes C-to-A cell fate transition, and that VEGF maintains the capillary fate by
269 counteracting the FSS-arterial program.
270 Importantly, VEGF inhibited the FSS-induced arterial program in a dose-dependent manner in
271 HMVBECs (Fig.4g). Among the arterial genes examined, Gja5 and Gja4 were most sensitive to VEGF
272 inhibition, as 2ng/ml VEGF was sufficient to completely inhibit FSS-induction of these genes (Fig.4g).
273 Moreover, blocking VEGF signaling by silencing PLCγ1 effectively rescued VEGF inhibition of the FSS-
274 arterial program (Fig.4h). Collectively, these data show that, during arterial specification, the transition
275 from capillary to arterial fate is regulated by VEGF-FSS competition (Fig.4i). VEGF serves as a
276 physiological brake to slow down FSS-driven arterial specification, thus maintaining the capillary bed
277 (Fig.4i).
278
279 **VEGF does not use Notch to counteract the FSS-induced arterial program.**
280 Notch signaling is an important arterial feature, but the requirement of Notch for arterial
281 specification has been under debate[9,13,16,31]. Since both VEGF and FSS are inducers of Notch signaling,
282 we sought to investigate the requirement of Notch for the FSS-arterial program and how VEGF
283 signaling interacts with this process. However, our data show that, although VEGF consistently
284 inhibited arterial genes (Fig.4d, e, g and Fig.5), its effects on FSS-induced Notch signaling was variable
285 in different experiments. In the presence of VEGF, FSS-induced notch intracellular domain (NICD) and
286 Dll4 protein were downregulated (Fig.4e) or upregulated (Fig.5, DMSO control). This observation
287 suggests that Notch signaling is not the mechanism that VEGF uses to inhibit the FSS-arterial program.
288 To test this hypothesis, we examined the FSS-induced arterial program on a background of Notch
289 inhibition. HMVBECs were pretreated with 5μM DAPT for 3h to eliminate Notch activity before applying
290 FSS. Unexpectedly, most arterial genes tested here were effectively induced by FSS under Notch
291 inhibition (Fig.5). The FSS induction of Sox17, Sema3G, and Jag1 with DAPT was at levels comparable
292 to those under control (DMSO) condition (Fig.5), indicating that these arterial genes are Notch-
293 independent. Efnb2, Gja5 and Gja4 were induced by FSS with DAPT, but at lower levels, indicating
294 partial dependence on Notch (Fig.5). FSS-induced Dll4 expression was largely compromised by Notch
295 inhibition, confirming its Notch-dependent feature (Fig.5). Thus, the FSS-arterial program involves
296 Notch-dependent and independent mechanisms. Notably, the inhibitory effect of VEGF on the FSS-
297 arterial program (Gja4, Gja5, Sox17, Sema3g, Efnb2 and Jag1) was well preserved with DAPT(Fig.5).
298 This finding confirms our hypothesis that VEGF does not use Notch signaling to suppress the FSS-
299 arterial program.
300 As constitutive Notch signaling is known to induce arterial genes[16], we wondered whether FSS
301 induces a persistent pattern of Notch activity in the arterial ECs. Using the Notch reporter mouse line
302 CBF:H2B-Venus[27] to examine endothelial Notch activity in neonatal retina, we found that 13.3%
303 Sox17^{high} arterial ECs did not colocalize with CBF-Venus nuclear signal, indicating undetectable Notch
304 activity in these arterial ECs (Supplemental Fig.8a). Next, we used HMVBECs to monitor the temporal
305 dynamic of FSS-induced Notch activity and its association with arterial gene induction. In contrast to the
306 expression of arterial genes (Jag1, Sox17, Efnb2, Sema3g) which showed a persistently increasing
307 pattern, FSS-induced NICD exhibited a pattern of fluctuation with two peaks at 1hr and 20hr,
308 respectively, and a valley of low activity between 3-9hr (Supplemental Fig.8b). These in vivo and in vitro
309 observations suggests that FSS does not rely on persistent Notch signaling to activate the arterial
310 program.
311 Notch inhibition leads to poor lumenization[32] and uncontrolled VEGF activity[19], a condition with low
312 FSS and high VEGF, both potentially compromise arterial specification. We wonder, in the context of
313 Notch inhibition, whether blocking VEGF signaling rescues arterialization. To this end, we used mice
314 with an endothelial knockout of Dll4 (*Dll4*^{iECKO}) as these mice consistently displayed a hypersprouting

vascular phenotype with completely compromised arteriogenesis (no Sox17^{high} ECs) and poor vascular patency (poor IB4 perfusion) (Supplemental Fig.8c). DC101 effectively rescued defective formation of major vessels and vascular perfusion in the *Dll4*^{iECKO} retinas (Supplemental Fig.8c). However, most of the major vessels in DC101-treated *Dll4*^{iECKO} retina exhibited wide diameter and a lack of Sox17^{high} staining (Supplemental Fig.8c). These observations indicate the requirement of Notch activity for arterial morphogenesis. In summary, the FSS-induced arterial program involves both Notch-dependent and independent mechanisms with VEGF utilizing a Notch-independent mechanism to inhibit the FSS-determined arterial fate.

Sox17 is the key mediator of the FSS-arterial program.

The uniform responses of arterial genes to FSS in the absence or presence of VEGF suggests a common transcription control point. Using the bioinformatic tool TRANSFAC to interrogate potential common transcription factors for arterial, Notch and capillary genes, we found predicted binding motifs of Sox17, a transcription factor indispensable for arterial specification[11], in the proximal promoters and/or the introns of all arterial and Notch genes, including Sox17 itself, but not in the capillary genes (Supplemental Table 2). Furthermore, most arterial genes, with the exception of Sox17 and Gja4, and some capillary genes share predicted binding motifs for Notch transcription regulator Rbpj (Supplemental Table 3). These findings suggest that Sox17 is a unique transcription regulator of the arterial program.

Since Sox17 is part of the arterial program induced by FSS (Fig.4), we used CRISPR cas9 to knockout Sox17 in HUVECs to verify whether Sox17 is required for the FSS-arterial program. The loss of Sox17 profoundly compromised the FSS-induced arterial program, resulting in almost no induction of Gja5, Gja4, Sema3g, Efnb2 and Nrp1 and reduced induction of Unc5b and Jag1 (Fig.6a). CRISPR cas9-mediated deletion of Sox18, another SoxF factor, exhibited only modest effect on the FSS induction of Gja4 and Efnb2 without affecting the rest of the FSS-arterial program tested here (Fig.6a). Combined knockout of Sox17 and Sox18 did not enhance the effect of Sox17 knockout alone on the FSS-arterial program (Fig.6a). At the same time, doxycycline (Dox)-inducible Sox17 overexpression in HUVECs effectively activated the arterial program at static condition in the absence of flow (Fig.6b). Importantly, there was a dose-dependent induction of Gja5, Gja4, Sema3g, Nrp1 and Jag1(Fig.6b). Taken together, these data establish Sox17 as the key mediator of the FSS-arterial program.

VEGF inhibits the arterial fate specification program by compromising Sox17 enrichment on arterial promoters and enhancers.

The data above implicate Sox17 as a key transcriptional regulator of the arterial fate specification program and makes it a likely target for VEGF signaling to inhibit this program. To test this, we first used the Dox-induced Sox17 expression system in HUVECs described above to examine the effect of VEGF on Sox17-induced arterial specification (Fig.7a). Our data show that VEGF effectively inhibited Sox17-activated transcription of the definitive arterial genes, including Gja5, Gja4, sema3g, Jag1, Cxcl12 and Efnb2 (Fig.7a). This result was not achieved by VEGF reducing Sox17 expression (Fig.7a). Importantly, the effect of VEGF suppression on Sox17-induced arterial program was dose-dependent (Fig.7b), which completely recapitulates the dose-dependent effect of VEGF on inhibiting the FSS-arterial program (Fig.4g). As a positive control of VEGF signaling, we examined the expression of non-specific arterial genes Unc5b and Dll4, two known VEGF-Notch targets enriched in both arterial and sprouting ECs (reference[3,33] and Supplemental Fig.6). As expected, Sox17-induced expression of Unc5b and Dll4 was further enhanced by VEGF (Fig.7a), proving a genuine effect of VEGF signaling in this experiment.

Since VEGF inhibition of the arterial program does not rely on reduction in Sox17 expression (Fig.7a-b, Supplemental Fig.7), we next tested whether VEGF affects Sox17's role as a transcription regulator on arterial promoters and recently reported arterial enhancers[34]. Chromatin immunoprecipitation (ChIP) assay was used to pull down Sox17-bound chromatin from HUVECs harboring Dox-inducible Sox17 expression system under the following conditions: no treatment (NT), Dox and Dox with VEGF (Fig.7c). Dox-induced Sox17 expression led to enrichment of Sox17 binding on arterial promoters and enhancers tested here, including the proximal promoters of Gja5, Gja4, Sema3g, Jag1, Cxcl12 and Efnb2, and arterial enhancers Gja5-7, Gja5-78, Gja4+50, Cxcl12+269 (Fig.7c), confirming the role of Sox17 as a transcription regulator in the arterial program. Critically, the enrichment of Sox17 was effectively suppressed by VEGF (Fig.7c). These findings in transcription regulation are in agreement with the effect of VEGF on Sox17-induced expression of the arterial program (Fig.7a).

Discussion

The key finding of our study is that VEGF-FSS crosstalk regulates arterial fate specification. Our data indicate that FSS is the principal driver of arteriogenesis, remodeling a pre-existing capillary bed into arterial vasculature. FSS achieves this effect by promoting the expression of Sox17, which binds to transcription regulatory elements in genes that induce the arterial fate specification program. VEGF antagonizes the FSS-dependent arterial program by limiting Sox17 enrichment at arterial promoters and enhancers. These findings explain the sequential nature of angiogenesis and arteriogenesis with VEGF-dependent formation of the capillary bed preceding the onset of arterial fate specification and the formation of morphologically identifiable arterial blood vessels. This finding also establishes the mechanism that prevents ectopic arteriogenesis and explains widespread failures of VEGF-driven "therapeutic angiogenesis" strategies.

Over the past decade, studies using lineage tracing have elucidated a sequence of well-coordinated processes that regulate vascular morphogenesis in the mouse neonatal retina (Fig 8a). Venous ECs proliferate, migrate against the blood flow and contribute to formation of the capillary bed and arteries[35,36] as do capillary ECs and tip cells[37,36]. By contrast, arterial ECs do not contribute to the endothelium of other vascular beds[37], suggesting that arterial fate is the final step in the vascular morphogenesis process (Fig.8a).

The entirety of this vascular morphogenesis process is guided by two major environmental cues: a gradient of VEGF, produced by the avascular, hypoxic neural bed, and the FSS, the hemodynamic force exerted on ECs by blood flow through lumenized vessels (Fig.8b). Whereas VEGF-guided sprouting angiogenesis expands the vasculature to meet the increasing demand for oxygen and nutrient supply during organogenesis, the FSS-driven arteriogenesis transforms parts of the capillary bed into arteries to accommodate the increasing volume of arterial blood (Fig.8b). In particular, artery-associated capillaries, extending ahead of the artery tip to the vascular front resemble a river delta that receive flow directly from the main artery (Fig.8b). This artery-associated capillary region, which we refer herein as "*arterial delta*", is subjected to sufficiently high FSS to drive arterialization (Fig.8b). At the same time, near the avascular zone, capillaries in the arterial delta region are exposed to high levels of VEGF (Fig.8b). Subjected to both VEGF and FSS, a portion of the arterial delta is remodeled into arteries, while the rest of the region is protected from ectopic arterialization and maintains its capillary identity (Fig.8b). The latter is critical, as excessive arterialization of the capillary bed would reduce the amount of microvasculature required for the effective exchange of oxygen, nutrient and metabolites. Therefore, a finely tuned mechanism is required for balancing arterialization and capillary bed maintenance during vascular morphogenesis.

407 Critically, both in vivo data from four independent experimental approaches and in vitro shear stress
408 experiments show that the FSS-induced arterial program does not require and is independent of
409 VEGFR2 signaling. Our data also clearly indicate that VEGF treatment does not induce arterial fate in
410 capillary ECs and that the FSS-induced arterial specification requires a permissive condition
411 characterized by declining VEGF/VEGFR2 signaling. These findings explain why arterial formation
412 occurs away from the vascular front, where high levels of VEGF protect capillaries from ectopic
413 arterialization. Based on these findings, we propose a novel paradigm: competing signals from VEGF
414 and FSS control the balance of angiogenesis, capillary maintenance and arteriogenesis (Fig.8c). During
415 vascular morphogenesis in the postnatal retina, tissue growth results in continuous expansion of the
416 avascular zone, where hypoxia induces high level of VEGF to trigger angiogenic sprouting (Fig.8b). As
417 the expanding capillary bed blood flow increases tissue oxygenation, hypoxia-induced VEGF
418 production declines (Fig.8b), creating a permissive condition for the rising FSS to drive capillary-to-
419 artery cell fate transition and ultimately the formation of new arteries. Thus, besides its role in
420 angiogenic sprouting, VEGF also maintains the capillary bed by serving as a physiological brake to
421 counteract the FSS-driven arterial program, which prevents the capillary bed from premature
422 arterialization.
423 In this study, we compared angiogenesis and arteriogenesis phenotypes in *Vegfa*^{iKO}, *Vegfr2*^{iECKO},
424 *Plcg1*^{iECKO} and DC101-treated mice, 4 different approaches to blocking VEGFR2 signaling (Fig.1,
425 Fig.8b). While each intervention led to partially distinct phenotypes, in all cases there was a reduction in
426 angiogenesis whereas arteriogenesis was maintained or even increased. In addition, in all cases there
427 was ectopic arterialization in the arterial delta region, leading to the disappearance of the un-arterialized
428 gap. DC101 treatment in particular led to a massive ectopic arterialization in the arterial delta region
429 (Fig.1d, Fig.8b). This likely reflects better preservation of the capillary bed, thereby allowing for more
430 capillary-to-artery fate transitions facilitated by the blockade of VEGFR2 signaling that left FSS-driven
431 arteriogenesis program unopposed (Fig.8b). Furthermore, while DC101 specifically blocks VEGF-
432 dependent activation of VEGFR2 signaling, it does not block ligand-independent functions of VEGFR2
433 such as mechanosensing and biological activities driven by its numerous co-receptors and partner
434 proteins such as VEGFR1, integrins, Nrp1, and Sdc2 among others[38-46]. In other words, *VEGFR2*^{iECKO}
435 potentially jeopardizes several essential signaling pathways, thereby directly or indirectly affecting the
436 extent of FSS-induced arterialization. Thus, severe vascular rarefaction in *Vegfa*^{iKO}, *Plcg1*^{iECKO} and
437 *VEGFR2*^{iECKO} mice likely interferes with normal heart development and/or function, reducing cardiac
438 output and resulting in insufficient FSS to drive full arterial specification. Severe vascular rarefaction in
439 these mice also potentially created uneven blood flow in the regressing capillary region, further
440 weakening the magnitude of the FSS. By contrast, the preservation of a substantial capillary bed in the
441 DC101-treated retinas, likely due to incomplete neutralizing effect to VEGFR2 as indicated by the
442 modest angiogenesis phenotype, possibly provides a “healthier” vascular environment with effective
443 level of FSS to take effect on arterialization. These findings also illustrate the need for effective
444 angiogenesis/arteriogenesis coupling[47] and the need for formation of the adequate capillary bed to
445 support effective arteriogenesis.
446 While the arterial vasculature in *Vegfa*^{iKO} and *Plcg1*^{iECKO} mice retinas show similar magnitudes of
447 Sox17^{high}-labeled arterial extension, there are distinct differences in the extent of smooth muscle
448 coverage in *Vegfa*^{iKO} compared to *Plcg1*^{iECKO} mice. This difference likely reflects a more profound
449 inhibition of VEGFR2 signaling in the absence of VEGF (*Vegfa*^{iKO}) than PLCγ1 deletion. Indeed,
450 although PLCγ1 knockout blocks the signaling from VEGFR2-Y1173, signaling from other tyrosine
451 phosphorylation sites of VEGFR2, such as Y951, Y1054, Y1059, Y1214, is retained. Furthermore, the
452 uncoupling of Sox17-driven arterial fate transition from arterial smooth muscle coverage in the *Vegfa*^{iKO}
453 retinas suggests defective pericyte physiology and EC-pericyte crosstalk, as a global loss of VEGF-A

also affects pericyte VEGFR1 signaling essential for normal pericyte biology[48,49]. Overall, the differences in morphological arterialization beyond the initial arterial specification step in these different animal experiments suggest that although VEGF serves as a physiological brake to slow down the FSS-driven arterial program, arterial morphogenesis requires formation of a capillary bed driven and maintained by VEGF.

Notch signaling is an essential feature of the arterial vasculature and has been proposed to be the central determinant of arterial specification. Intriguingly, the combination of VEGF and FSS, two well-known Notch inducers, does not have an additive effect on arterial specification. Our data show that FSS induction of some definitive arterial genes (e.g. Sox17 and Sema3G) is independent of Notch signaling, while others (e.g. Gja4, Gja5 and Dll4) are at least partially dependent on Notch. Therefore, FSS relies on both Notch-dependent and -independent mechanisms to induce arterial genes expression. It is possible that Notch contributes to arterial specification mainly by inhibiting cell cycle progression, a prerequisite for the FSS-induced arterial program[16,50].

Importantly, our data show that VEGF does not use Notch to antagonize the arterial program, as Notch inhibition does not affect this mechanism. Instead, Sox17 is the central mediator of the FSS-arterial program. Members of the SoxF family of transcription factors, Sox7, Sox17 and Sox18, are expressed by all ECs[51], but only Sox17 is enriched in the arterial ECs and is implicated in arterial specification[11,51]. Our data show that Sox17 is not only a critical transcription activator for the FSS-arterial program but also serves as a target for VEGF signaling to counteract the FSS-arterial program, because VEGF signaling compromises SOX17 binding to arterial promoters and enhancers.

Arterial morphogenesis involves not only fate specification to acquire arterial identity, but also a process of cell migration and vascular coalescence to form major arterial vessels. Our proposed model of VEGF-FSS competition on arterial specification is in line with a recent report showing that VEGF-FSS interaction modulates EC polarity and migration during capillary remodeling[52]. However, it remains unclear whether the acquisition of arterial gene expression determines cell migration behavior when remodeling the capillary bed into a main artery. The mechanistic association between arterial differentiation and migration requires further investigation to elucidate.

Taken together, our data support a new understanding of arteriogenesis that involves the primacy of the FSS signaling and the FSS-VEGF crosstalk. Transient, well controlled VEGF stimulation is necessary for the formation of the capillary bed that is then partially remodeled into the arterial vasculature. The latter step, however, requires cessation of VEGF signaling. These findings have direct therapeutic consideration for vascular revascularization approaches.

Methods

Animal studies

Vegfr2$^{flox/flox}$ mice (a gift kindly provided by Lena Claesson-Welsh, Uppsala University), *Plcg1*$^{flox/flox}$ mice (a gift kindly provided by Renren Wen, Wisconsin Blood Institute) and *Dll4*$^{flox/flox}$ mice (a gift kindly provided by Prof. Bin Zhou, Albert Einstein College of Medicine) were crossed with *Cdh5CreER*^{T2} mice (a gift kindly provided by Ralf Adams). *CBF:H2B-Venus* mice, purchased from Jackson Laboratory, were crossed with *Vegfr2*$^{flox/flox}$*; Cdh5CreER*^{T2} *mice and Plcg1*$^{flox/flox}$*; Cdh5CreER*^{T2} *mice*, respectively. *Vegf2*$^{flox/flox}$*; Cdh5CreER*^{T2} mice were in *C57Bl/6J* background. *Plcg1*$^{flox/flox}$*; Cdh5CreER*^{T2} *mice were backcrossed to C57Bl/6J* background for 10 generations. Gene deletion was induced by three consecutive dosages of 100μg Tamoxifen via daily peritoneal injection. Tamoxifen powder (Sigma, T5648) was suspended in corn oil (Sigma, C8267) and then dissolved by agitation at 37°C for 2 hours(hrs). Rat IgG or DC101 antibody was injected peritoneally at postnatal day 1 (400μg) and 3 (200μg). All aforementioned mouse experimental procedures complied to the protocols approved by the Yale University Institutional Animal Care and Use Committee (IACUC). Genotyping primers are listed in

501 Supplemental Table 4. The following study was performed at the UCL Institute of Ophthalmology
502 following UK Home Office and institutional Animal Welfare and Ethical Review Body (AWERB)
503 guidelines. Mice carrying the *Vegfa*$^{fl/fl}$ alleles[53] maintained on a mixed genetic background (C57BL6/J
504 and 129/Sv) were crossed with *Vegfa*$^{fl/fl}$ mice carrying a tamoxifen-inducible *Cre* transgene under the
505 control of the ubiquitous chicken actin promoter (CAG-CreER^{TM})[54]. *Vegfa*$^{fl/fl}$ littermate pups expressing
506 or lacking CAG-CreER^{TM} received intraperitoneal injections of 50 µg tamoxifen on postnatal days (P) 2
507 and P4.
508
509 **Retinal dissection**
510 Mouse neonates were euthanized at postnatal day 1(P1) to 6(P6). Eyes were enucleated and
511 immediately fixed with 4% paraformaldehyde (PFA) for 8 minutes (min) at room temperature (RT). Then
512 the eyes were transferred to PBS to terminate pre-dissection fixation. Dissected retinas were fixed with
513 4% paraformaldehyde for 30 min at RT with gentle rocking, followed by 2 washes in PBS at RT, 10 min
514 each. Then retinas were dehydrated in methanol and stored at -20°C for subsequent procedure. Before
515 immunostaining, retinas stored in methanol were warmed up at room temperature and rehydrated with
516 PBS.
517
518 **Immunostaining and confocal imaging**
519 Retinas were incubated in wash buffer (PBS with 0.1%Triton X100) with gentle rocking for 15 min
520 and then in blocking buffer (wash buffer with 5% normal donkey serum (Jackson ImmunoResearch,
521 017-000-121)) for 1-2 hrs. Blocked retinas were incubated with primary antibodies diluted in blocking
522 buffer overnight at 4°C with gentle rocking. On the next day, the retinas were washed in wash buffer for
523 3 times, 15 min each. Secondary antibodies were mixed with isolectin B4 in blocking buffer for staining
524 at RT for 1.5 h with gentle rocking in dark. Staining procedure was finished after 3 washes in wash
525 buffer, 15 min each. The retinas were transferred to PBS without detergent before flat mount to slides.
526 Antibodies and experimental conditions were listed in Supplemental Table 5. Image acquisition was
527 conducted with Leica TCS SP8 Confocal Laser Scanning Microscope. Leica LAS-X, Image J (NIH) and
528 IMARIS (Bitplane, USA) were used for image analysis.
529
530 **EdU labeling**
531 50ug EdU (Sigma #900684) solution were peritoneally injected into mouse neonates at P5 4h
532 before retinal dissection. Erg antibody (Abcam, # ab214341) was stained to visualize endothelial nuclei,
533 followed by detection of EdU incorporation using EdU Cell Proliferation Kit (Invitrogen, #C10340).
534
535 **Immunostaining of phospho-ERK1/2**
536 Mouse neonates at P5 were placed on a warm pad at 37°C for 30min. The eyes were enucleated
537 and immediately fixed in 4% PFA for 8 min, RT. Using ice-cold PFA will decrease fixation efficacy and
538 must be avoided at this step. The retinas were then transferred to and dissected in ice-cold PBS. Post-
539 dissection fixation in 4% PFA was done at 4°C with gentle rocking for 2 h. The fixed retinas were
540 washed once with PBS for 5min, RT, and stored in ice-cold methanol at -20°C for 1 h. After warming up
541 at RT for 15min, the retinas were rehydrated in PBS for 5min, followed by incubation in PBST (PBS
542 with 0.25%Triton X100) for 30min and then blocking in PBST with 10% normal donkey serum (blocking
543 buffer) for 1hr, RT. Phospho-p44/42 MAPK (Erk1/2) (Thr202/Tyr204) antibody (Cell signaling
544 Technology, #9101) were diluted 1:100 in blocking buffer. From this step, the staining procedure
545 followed the regular protocol described above.
546
547 **Vascular perfusion assay**

548 Mouse neonates at P5 or P6 were placed on a warm pad at 37°C for subsequent procedure of
549 vascular perfusion. IB4-Alexa488 was diluted in PBS and retro-orbitally injected to visualize patent
550 (lumenized) vessels. Calculation of IB4 dilution (1:50) was based on estimated blood volume
551 5.5ml/100g body weight (The Jackson Laboratory). 1:50= (IB4 volume) : (blood volume + injection
552 volume). Injected pups were placed on warm pad for 20min before dissection. Dissected retinas were
553 counter-stained with IB4-Alexa 647 to visualize all vessels, lumenized and unlumenized.
554
555 **Endothelial cell culture and flow (shear stress) systems**
556 Human microvascular blood endothelial cells (HMVBECs) (HDBECs, Promocell, #C-12211) were
557 maintained in EGM2-MV full growth medium (Lonza). EBM2 basal medium with 5% FBS, here we term
558 *permissive arterial differentiation medium (PADM5)*, was used for flow-induced arterial differentiation.
559 Approximately 6 h prior to start of flow, EGM2-MV medium was removed, followed by a wash and a
560 refill with PADM5. Human Umbilical Vein Endothelial Cells (HUVECs) (from Yale VBT) were maintained
561 in M199 medium containing 20%FBS and endothelial cell growth supplements (ECGS, aliquots of
562 Corning product were purchased from Yale VBT). For HUVECs, the maintenance medium was used for
563 flow-induced arterial differentiation.
564 HMVBECs or HUVECs were seeded in IBIDI μ-slides (0.4 Luer ibiTreat) (IBIDI, #80176), with an
565 initial seed density of 0.15x 10^6 (HMVBECs) or 0.12x 10^6 (HUVECs) cells per slide and were maintained
566 for 48 h in the slide channel to reach a monolayer of homeostasis before flow experiment.
567 Flow system was built with a mini peristaltic pump (Cole Parmer MasterFlex Peristaltic Pump C/L
568 drive P/N: 77122-22), an assembly of tubing systems with a syringe pulse dampener and a medium
569 reservoir. The tubing system was assembled with a coiled inlet tubing (60cm) and a coiled outlet tubing
570 (160cm), a total length of 220cm to further dampen pulsation. To avoid cell detachment, the end of the
571 outlet tubing was fit into the pump head to passively draw the flow out of the IBIDI channel instead of
572 pumping in. A flow rate of 12ml/min, which creates 12 dynes/cm^2 shear stress according to the IBIDI
573 manual, was accurately measured in each flow system prior to the start of flow experiment. Before
574 connecting IBIDI μSlides, the flow systems were placed in cell culture incubator for 30min for
575 equilibrium of temperature and CO_2.
576 To harvest cells from IBIDI μSlides for RNA or protein analysis, 150μl lysis buffer was added into
577 the channel, followed by a freezing-thawing cycle to facilitate cell lysing. To collect cell lysate from the
578 channel, approximately 75μl of thawed lysate was removed in order to create room for liquid movement.
579 Then the slide was gently tilted 10-15 times to make the rest cell lysate moving through the channel
580 back and forth. After collecting the rest cell lysate, 50ul of new lysis buffer was added into the channel
581 and then passed through repeatedly by gentle tilting to rinse off the residual cell lysate. A total of 200ul
582 cell lysate was collected from each channel.
583
584 **Small interfering RNA (siRNA) experiments**
585 FuGene SI transfection reagent (VWR, # MSPP-SI-1000) was used for siRNA transfection for lower
586 toxicity. HUVECs or HMVBECs were seeded in maintenance medium to reach a density of 80-90% on
587 the day of transfection. siRNA/FuGene/OptiMEM mix was added to EGM2-MV full growth medium for
588 6h, followed by a wash with PBS and replacement with fresh EGM2-MV full medium. On the next day,
589 the siRNA-treated cells were trypsinized and seeded in IBIDI μSlides with maintenance medium. Flow
590 experiments started at 72h after siPLCγ1 transfection. siRNA information is listed in Supplemental
591 Table 6.
592
593 **RNA isolation and RT-qPCR**

Qiagen RNeasy plus Mini kit (#74134) was used for total RNA isolation, followed by reverse transcription to synthesize cDNA using iScript cDNA Synthesis Kit (Bio-Rad, #170–8891). SYBR Green Supermix (Bio-Rad, #1798880) was used for qPCR. Cycle threshold (Ct) values of gene expression were subtracted from average housekeeping gene GAPDH, and relative quantification of experimental groups versus control was calculated. QPCR primers are listed in Supplemental Table 7.

RNA sequencing and bioinformatic analysis

Total RNA samples were sent to Yale Center for Genomic Analysis (YCGA) for quality analysis, library preparation and sequencing. Partek Flow was used for bioinformatic analysis. Briefly, adapters in RNAseq reads were trimmed, and the trimmed reads were aligned to aligner algorithm STAR. Normalized gene counts were analyzed using DESeq2 to determine differential gene expression.

Computational methods and cSTAR analysis.

To analyze EC responses to FSS, VEGF and a combined FSS plus VEGF, the control condition is selected as no treatment, static condition (ST) and the log fold-changes of the differentially expressed genes with respect to ST were calculated. The SVM algorithm with a linear kernel from the scikit-learn python library was applied to build a maximum margin hyperplane that distinguishes four different EC states. The STVs are calculated as unit vectors, which are normal vectors to the three hyperplanes separating EC states. After building the STVs, cSTAR calculates quantitative indicators of cell phenotypic states termed DPDs. The DPD scores describe the changes in the cell phenotypic features that would occur when the data point crosses on the separating hyperplanes. The absolute value of the DPD score is determined by the Euclidean distances from the data point to the separating hyperplane, while the sign of the DPD score indicates if the direction of the data point movement to cross the hyperplane is parallel or antiparallel to the corresponding STV[29]. The DPD scores were normalized so that the DPD values in the training set (FSS, VEGF, and FSS-VEGF states) were -1, 0 or 1. All codes of building STVs and calculating the normalized DPD scores will be provided in a journal publication.

Isolation of mouse retinal endothelial cell and scRNAseq

Retinas of control and *PLCγ1*^{iECKO} pups at p6 were dissected in ice-cold PBS. Dissected retinas from 3 control and 3 *PLCγ1*^{iECKO} pups, respectively, were pooled and subjected to magnetic-activated Cell sorting (MACS). Briefly, pooled retinal tissue was dissociated using Neural Tissue Dissociation kit (P) (Miltenyi Biotec, Cat#130- 092-628) with gentleMACS Dissociator (Miltenyi Biotec, Cat#130- 093-235). Isolated cells were suspended in PBS with 0.4% ultra-pure BSA as single cell suspension, which was subsequently incubated with CD31 MicroBeads (Miltenyi Biotec, Cat#130-097-418) for 30 min at 4°C with gentle rotation followed by passing through MS columns (Miltenyi Biotec, Cat#130-042-201) on an OctoMACS Separator (Miltenyi Biotec, Cat#130-042-109) to enrich endothelial cells.

Single cell suspensions were submitted to Yale Center for Genomic Analysis (YCGA) for library preparation and sequencing. scRNAseq libraries were created using Chromium GEM-X Single Cell 3′ Reagent Kits v4 (10x Genomics). Libraries were sequenced in NovaSeq HiSeq paired-end.

Reads alignment and UMI counting were conducted using the Cell Ranger software suite, with the mm10 genome assembly utilized for alignment[55]. Downstream analyses, including quality control (QC) filtering, batch correction, clustering, UMAP visualization, cell cycle analysis, and gene expression analysis, were performed in R using Seurat v5.1[56]. For quality control, cells with mitochondrial gene content exceeding 5% were excluded. Additionally, only cells with fewer than 100,000 total counts and between 200 and 9,000 detected features were retained for analysis. Counts normalization was executed using the Pearson residuals method implemented in the sctransform package[57]. Batch correction and data integration were carried out using the RPCA approach available in Seurat

package[56]. TSCAN method was employed for pseudotime trajectory analysis[58]. For RNA Velocity Analysis, splicing-specific counts were generated using the velocyto.py package[59]. For downstream processing of splicing data, the velocyto.R and Seurat-Wrappers packages were utilized[59]. Vector field plotting was conducted using the veloviz package[60] to visualize RNA velocity dynamics.

To access endothelial deletion of Plcg1, the brain tissue of control and *PLCγ1*^{iECKO} pups were used to isolate ECs. Brain ECs were first enriched by MACS as described above, then CD31+/CD45-/PI- ECs were specifically sorted out by fluorescence activated cell sorting (FACS) for RNA isolation and RT-PCR. The FACS-related antibodies are summarized in Supplemental Table 5. Deletion of Plcg1 in *PLCγ1*^{iECKO} ECs is evidenced in Supplemental Fig.4, which demonstrates the deletion of LoxP-flanked exons2-4 and the presence of a truncated Plcg1 mRNA with the downstream exons (Supplemental Fig.4b). This explains the observation of no detectable decrease of Plcg1 mRNA in the *PLCγ1*^{iECKO} ECs in scRNAseq analysis (Supplemental Fig.4c), as Chromium GEM-X Single Cell 3′ Reagent Kits v4 uses the poly(dT) primers that capture the polyA sequences of mRNA and generates cDNA libraries with downstream sequences at the 3' end, similar to a recent scRNAseq study with the same issue to detect gene deletion[61].

Western blots

The following recipe (kindly provided by Prof. Jannifer Fang, Tulane University) was used to prepare 10ml lysis buffer for detecting Connexins (Gja4 and Gja5) and also workable for other proteins. A tablet of protease inhibitor cocktail (Roche) and a tablet of PhosSTOP were dissolved in 4.75ml water. Then the following reagents were sequentially added and then mixed: 1.25ml 1M Tris, 2ml 20%SDS, 2ml Glycerol, 1ml beta-mercaptoethanol and a tip amount of blumophenol blue. At the end of flow experiment, IBIDI μSlides were detached from the flow system and placed on ice. To harvest protein lysate from IBIDI μSlide, medium was vacuum removed from the channel and replaced with 150ul lysis buffer. To enhance protein lysing, the IBIDI μSlide with lysis buffer was subject to a freezing-thawing cycle. Subsequently, with the removal and collection of 50% lysis buffer to create room for movement in the channel, the slide was repeatedly tilted several times to create shear force to enhance protein extraction before collecting the rest protein lysate. An additional 50ul of new lysis buffer was pipetted into the channel to rinse and collect any residual protein lysate, making a total volume of 200ul. Protein lysate was collected in a centrifuge tube and sonicated for 1 min at 15% power, followed by heating at 75°C for 30 min to denature protein. Antibodies used for western blot were listed in Supplemental Table 8.

Doxycycline-induced Sox17 expression and induction of arterial differentiation

Doxycycline-inducible Sox17 expression lentiviral construct pCW57.1-hSox17-DDK-Myc was created in the Simons lab and can be shared upon reasonable request. Maintained in the aforementioned M199-based media (M199 supplemented with 20%FBS and ECGS), HUVECs at passage 2-3 were used for Lentiviral transduction, during which EGM2-MV media was temporarily used to replace M199-based media to enhance transduction efficiency and cell survival. Transduced HUVECs were selected by 0.8ug/ml puromycin in EGM2-MV media for 48 hours, followed by a 48-hour window of recovery. Puromycin-selected, transduced HUVECs were either frozen for future experiments or seeded in M199-based media for subsequent arterial differentiation experiments.

To induce arterial differentiation, 1.9-2.0 x 10^6 HUVECs harboring pCW57.1-hSox17 were seeded in M199-based media in each 10-cm dish on day1, which ensures the formation of a confluent endothelial monolayer for the start of doxycycline treatment on the next day (day2). Fresh media with doxycycline was replaced once on day3. The cells were harvested at the end of a 48-hour treatment on day4.

To ensure consistent and reproducible results, HUVECs must be regularly maintained in M199-based medium instead of EGM2, with final passage no more than 6 at the end of arterial differentiation.

Chromatin Immunoprecipitation (ChIP)

ChIP assays were conducted using SimpleChIP Plus Enzymatic Chromatin IP kit (Cell Signaling Tech #9005) following the official protocol. Briefly, HUVECs in a 10-cm dish were fixed with ultra-pure formadehyde (methanol free) (Polysciences, 18814-10) to create protein-chromatin crosslink. Immunoprecipitation was performed with antibody targeting Sox17 (CST#81778) and control rabbit IgG (CST#2729). Pull-downed chromatin was eluted, purified and assayed by QPCR.

CRISPR-cas9-mediated gene deletion

Oligos of designed gRNA sequences were cloned into lentiCRISPRv2 (Addgene #52961) following previously published protocol[62]. The following gRNA sequences were used, including a non-targeting gRNA (GTATTACTGATATTGGTGGG), a pair of gRNAs targeting human Sox17 (ACGGGTAGCCGTCGAGCGG and GGCACCTACAGCTACGCGC)[63], and a gRNA targeting human Sox18 (GTGGAAGGAGCTGAACGCGG). HUVECs transduced with lentiviral-delivered sgRNAs were selected with 0.8ug/ml puromycin for 48hrs and maintained in EGM2-MV medium for 7 days to ensure sufficient gene recombination. This was followed by a second cycle of selection with puromycin for 48hrs and recovery for 3 days before seeding the cells to the IBIDI μ slides for flow experiments.

Statistics

Data was plotted and analyzed using GraphPad Prism10. Student's t test was used for comparison of two groups, with the assumption of normal distribution and equal variance between groups. One-way or two-way ANOVA with multiple comparisons was used for grouped samples on one or two variables. A p value equal to or less than 0.05 was determined as statistically significant.

Author contributions

DC, MS and MAS conceptualized and designed the project. DC conducted and analyzed most of the experiments. MS and MAS supervised the project. DC and MS wrote the manuscript with edits from MAS, CR and KAM. OSR, DC, AT, BNK analyzed the scRNAseq data. DC analyzed the RNAseq data. OSR and BNK conducted the cSTAR analysis based on the RNAseq data. DJ and BGC contributed to the shear stress experiments and cloning the CRISPR-Cas9 system for Sox17 deletion and provided technical assistance to DC creating the lentiviral construct of Sox17 expression. DC and RC designed and conducted the Sox17 ChIP experiments with KAM's supervision. MR and EI conducted the experiments of the VEGF knockout mice with CR's supervision.

Acknowledgements

We thank Prof. Lena Claesson-Welsh, Prof. Ralf Adams, Prof. Renren Wen and Genentech for providing the *VEGFR2*$^{flox/flox}$, the *Cdh5CreER*^{T2}, the *PLCγ1*$^{flox/flox}$ and the *Vegfa*$^{flox/flox}$ mice, respectively. We thank Dr. Hyojin Park and Dr. Eunate Gallardo for essential technical support in sample preparation for single cell RNA sequencing. Sequencing service by Yale Center for Genomic Analysis reported in this publication was supported by the National Institute of General Medical Sciences of the National Institutes of Health under Award Number 1S10OD030363-01A1. We thank Drs. Prajwal Boddu, Emma Ristori and Federico Corti for technical advice on cloning. We thank Rolando Milian, Yale Medical Library, for bioinformatic training and assistance of RNAseq data analysis. We thank Tuo Guo and Guilherme Dantas for technical assistance in immunostaining, confocal imaging and cloning. This work was supported by NIH grants R01HL169520-01 (MS), P01HL107205-06A1 (MS and MAS), NIH/NCI

grant R01CA244660 (BNK), EU grant no. 101136926 MULTIR (BNK), Science Foundation Ireland 22/PATH-S/10875 (OSR) and Open Philanthropy (MS), British Heart Foundation PG.23.11342 (CR and MR) and PG.24.11119 (CR).

739 **Reference**
740

741 1 Simons, M. & Eichmann, A. Molecular controls of arterial morphogenesis. *Circ Res* **116**, 1712-
742 1724, doi:10.1161/CIRCRESAHA.116.302953 (2015).
743 2 Wythe, J. D. *et al.* ETS factors regulate Vegf-dependent arterial specification. *Dev Cell* **26**, 45-
744 58, doi:10.1016/j.devcel.2013.06.007 (2013).
745 3 Lobov, I. B. *et al.* Delta-like ligand 4 (Dll4) is induced by VEGF as a negative regulator of
746 angiogenic sprouting. *Proc Natl Acad Sci U S A* **104**, 3219-3224, doi:10.1073/pnas.0611206104
747 (2007).
748 4 Liu, Z. J. *et al.* Regulation of Notch1 and Dll4 by vascular endothelial growth factor in arterial
749 endothelial cells: implications for modulating arteriogenesis and angiogenesis. *Mol Cell Biol* **23**,
750 14-25, doi:10.1128/MCB.23.1.14-25.2003 (2003).
751 5 Hellstrom, M. *et al.* Dll4 signalling through Notch1 regulates formation of tip cells during
752 angiogenesis. *Nature* **445**, 776-780, doi:10.1038/nature05571 (2007).
753 6 Kopan, R. & Ilagan, M. X. The canonical Notch signaling pathway: unfolding the activation
754 mechanism. *Cell* **137**, 216-233, doi:10.1016/j.cell.2009.03.045 (2009).
755 7 Ubezio, B. *et al.* Synchronization of endothelial Dll4-Notch dynamics switch blood vessels from
756 branching to expansion. *Elife* **5**, doi:10.7554/eLife.12167 (2016).
757 8 Hasan, S. S. *et al.* Endothelial Notch signalling limits angiogenesis via control of artery
758 formation. *Nat Cell Biol* **19**, 928-940, doi:10.1038/ncb3574 (2017).
759 9 Lawson, N. D. *et al.* Notch signaling is required for arterial-venous differentiation during
760 embryonic vascular development. *Development* **128**, 3675-3683, doi:10.1242/dev.128.19.3675
761 (2001).
762 10 Roca, C. & Adams, R. H. Regulation of vascular morphogenesis by Notch signaling. *Genes Dev*
763 **21**, 2511-2524, doi:10.1101/gad.1589207 (2007).
764 11 Corada, M. *et al.* Sox17 is indispensable for acquisition and maintenance of arterial identity. *Nat*
765 *Commun* **4**, 2609, doi:10.1038/ncomms3609 (2013).
766 12 Benedito, R. *et al.* Loss of Notch signalling induced by Dll4 causes arterial calibre reduction by
767 increasing endothelial cell response to angiogenic stimuli. *BMC Dev Biol* **8**, 117,
768 doi:10.1186/1471-213X-8-117 (2008).
769 13 Pitulescu, M. E. *et al.* Dll4 and Notch signalling couples sprouting angiogenesis and artery
770 formation. *Nat Cell Biol* **19**, 915-927, doi:10.1038/ncb3555 (2017).
771 14 Zarkada, G., Heinolainen, K., Makinen, T., Kubota, Y. & Alitalo, K. VEGFR3 does not sustain
772 retinal angiogenesis without VEGFR2. *Proc Natl Acad Sci U S A* **112**, 761-766,
773 doi:10.1073/pnas.1423278112 (2015).
774 15 Red-Horse, K. & Siekmann, A. F. Veins and Arteries Build Hierarchical Branching Patterns
775 Differently: Bottom-Up versus Top-Down. *Bioessays* **41**, e1800198,
776 doi:10.1002/bies.201800198 (2019).
777 16 Fang, J. S. *et al.* Shear-induced Notch-Cx37-p27 axis arrests endothelial cell cycle to enable
778 arterial specification. *Nat Commun* **8**, 2149, doi:10.1038/s41467-017-01742-7 (2017).
779 17 Masumura, T., Yamamoto, K., Shimizu, N., Obi, S. & Ando, J. Shear stress increases
780 expression of the arterial endothelial marker ephrinB2 in murine ES cells via the VEGF-Notch
781 signaling pathways. *Arterioscler Thromb Vasc Biol* **29**, 2125-2131,
782 doi:10.1161/ATVBAHA.109.193185 (2009).
783 18 Kim, D. *et al.* Sox17 mediates adult arterial endothelial cell adaptation to hemodynamics.
784 *Biomaterials* **293**, 121946, doi:10.1016/j.biomaterials.2022.121946 (2023).
785 19 Pontes-Quero, S. *et al.* High mitogenic stimulation arrests angiogenesis. *Nat Commun* **10**, 2016,
786 doi:10.1038/s41467-019-09875-7 (2019).
787 20 Gerhardt, H. *et al.* VEGF guides angiogenic sprouting utilizing endothelial tip cell filopodia. *J*
788 *Cell Biol* **161**, 1163-1177, doi:10.1083/jcb.200302047 (2003).
789 21 Stahl, A. *et al.* The mouse retina as an angiogenesis model. *Invest Ophthalmol Vis Sci* **51**,
790 2813-2826, doi:10.1167/iovs.10-5176 (2010).

22 Okabe, K. *et al.* Neurons limit angiogenesis by titrating VEGF in retina. *Cell* **159**, 584-596, doi:10.1016/j.cell.2014.09.025 (2014).
23 Takahashi, T., Yamaguchi, S., Chida, K. & Shibuya, M. A single autophosphorylation site on KDR/Flk-1 is essential for VEGF-A-dependent activation of PLC-gamma and DNA synthesis in vascular endothelial cells. *EMBO J* **20**, 2768-2778, doi:10.1093/emboj/20.11.2768 (2001).
24 Chen, D. & Simons, M. Emerging roles of PLCgamma1 in endothelial biology. *Sci Signal* **14**, doi:10.1126/scisignal.abc6612 (2021).
25 Kilarski, W. W., Samolov, B., Petersson, L., Kvanta, A. & Gerwins, P. Biomechanical regulation of blood vessel growth during tissue vascularization. *Nat Med* **15**, 657-664, doi:10.1038/nm.1985 (2009).
26 Tong, R. T. *et al.* Vascular normalization by vascular endothelial growth factor receptor 2 blockade induces a pressure gradient across the vasculature and improves drug penetration in tumors. *Cancer Res* **64**, 3731-3736, doi:10.1158/0008-5472.CAN-04-0074 (2004).
27 Nowotschin, S., Xenopoulos, P., Schrode, N. & Hadjantonakis, A. K. A bright single-cell resolution live imaging reporter of Notch signaling in the mouse. *BMC Dev Biol* **13**, 15, doi:10.1186/1471-213X-13-15 (2013).
28 Kholodenko, B. N., Kolch, W. & Rukhlenko, O. S. Reversing pathological cell states: the road less travelled can extend the therapeutic horizon. *Trends Cell Biol* **33**, 913-923, doi:10.1016/j.tcb.2023.04.004 (2023).
29 Rukhlenko, O. S. *et al.* Control of cell state transitions. *Nature* **609**, 975-985, doi:10.1038/s41586-022-05194-y (2022).
30 Yabaji, S. M. *et al.* Cell state transition analysis identifies interventions that improve control of Mycobacterium tuberculosis infection by susceptible macrophages. *Sci Adv* **9**, eadh4119, doi:10.1126/sciadv.adh4119 (2023).
31 Luo, W. *et al.* Arterialization requires the timely suppression of cell growth. *Nature* **589**, 437-441, doi:10.1038/s41586-020-3018-x (2021).
32 Noguera-Troise, I. *et al.* Blockade of Dll4 inhibits tumour growth by promoting non-productive angiogenesis. *Nature* **444**, 1032-1037, doi:10.1038/nature05355 (2006).
33 Raza, Q. *et al.* Notch signaling regulates UNC5B to suppress endothelial proliferation, migration, junction activity, and retinal plexus branching. *Sci Rep* **14**, 13603, doi:10.1038/s41598-024-64375-z (2024).
34 Nornes, S., Bruche, S., Adak, N., McCracken, I. & Val, S. D. A catalogue of verified and characterized arterial enhancers for key arterial identity genes. *bioRxiv*, 2024.2004.2030.591717, doi:10.1101/2024.04.30.591717 (2024).
35 Lee, H. W. *et al.* Role of Venous Endothelial Cells in Developmental and Pathologic Angiogenesis. *Circulation* **144**, 1308-1322, doi:10.1161/CIRCULATIONAHA.121.054071 (2021).
36 Xu, C. *et al.* Arteries are formed by vein-derived endothelial tip cells. *Nat Commun* **5**, 5758, doi:10.1038/ncomms6758 (2014).
37 Park, H. *et al.* Defective Flow-Migration Coupling Causes Arteriovenous Malformations in Hereditary Hemorrhagic Telangiectasia. *Circulation* **144**, 805-822, doi:10.1161/CIRCULATIONAHA.120.053047 (2021).
38 Corti, F. *et al.* N-terminal syndecan-2 domain selectively enhances 6-O heparan sulfate chains sulfation and promotes VEGFA(165)-dependent neovascularization. *Nat Commun* **10**, 1562, doi:10.1038/s41467-019-09605-z (2019).
39 Cudmore, M. J. *et al.* The role of heterodimerization between VEGFR-1 and VEGFR-2 in the regulation of endothelial cell homeostasis. *Nat Commun* **3**, 972, doi:10.1038/ncomms1977 (2012).
40 Kendall, R. L., Wang, G. & Thomas, K. A. Identification of a natural soluble form of the vascular endothelial growth factor receptor, FLT-1, and its heterodimerization with KDR. *Biochem Biophys Res Commun* **226**, 324-328, doi:10.1006/bbrc.1996.1355 (1996).
41 Rahimi, N., Dayanir, V. & Lashkari, K. Receptor chimeras indicate that the vascular endothelial growth factor receptor-1 (VEGFR-1) modulates mitogenic activity of VEGFR-2 in endothelial cells. *J Biol Chem* **275**, 16986-16992, doi:10.1074/jbc.M000528200 (2000).

42 Dixelius, J. *et al.* Ligand-induced vascular endothelial growth factor receptor-3 (VEGFR-3) heterodimerization with VEGFR-2 in primary lymphatic endothelial cells regulates tyrosine phosphorylation sites. *J Biol Chem* **278**, 40973-40979, doi:10.1074/jbc.M304499200 (2003).
43 Shay-Salit, A. *et al.* VEGF receptor 2 and the adherens junction as a mechanical transducer in vascular endothelial cells. *Proc Natl Acad Sci U S A* **99**, 9462-9467, doi:10.1073/pnas.142224299 (2002).
44 Coon, B. G. *et al.* Intramembrane binding of VE-cadherin to VEGFR2 and VEGFR3 assembles the endothelial mechanosensory complex. *J Cell Biol* **208**, 975-986, doi:10.1083/jcb.201408103 (2015).
45 Tzima, E. *et al.* A mechanosensory complex that mediates the endothelial cell response to fluid shear stress. *Nature* **437**, 426-431, doi:10.1038/nature03952 (2005).
46 Somanath, P. R., Malinin, N. L. & Byzova, T. V. Cooperation between integrin alphavbeta3 and VEGFR2 in angiogenesis. *Angiogenesis* **12**, 177-185, doi:10.1007/s10456-009-9141-9 (2009).
47 le Noble, F. & Kupatt, C. Interdependence of Angiogenesis and Arteriogenesis in Development and Disease. *Int J Mol Sci* **23**, doi:10.3390/ijms23073879 (2022).
48 Eilken, H. M. *et al.* Pericytes regulate VEGF-induced endothelial sprouting through VEGFR1. *Nat Commun* **8**, 1574, doi:10.1038/s41467-017-01738-3 (2017).
49 Donoghue, L., Tyburski, J. G., Steffes, C. P. & Wilson, R. F. Vascular endothelial growth factor modulates contractile response in microvascular lung pericytes. *Am J Surg* **191**, 349-352, doi:10.1016/j.amjsurg.2005.10.034 (2006).
50 McDonald, A. I. *et al.* Endothelial Regeneration of Large Vessels Is a Biphasic Process Driven by Local Cells with Distinct Proliferative Capacities. *Cell Stem Cell* **23**, 210-225 e216, doi:10.1016/j.stem.2018.07.011 (2018).
51 Zhou, Y., Williams, J., Smallwood, P. M. & Nathans, J. Sox7, Sox17, and Sox18 Cooperatively Regulate Vascular Development in the Mouse Retina. *PLoS One* **10**, e0143650, doi:10.1371/journal.pone.0143650 (2015).
52 Barbacena, P. *et al.* Competition for endothelial cell polarity drives vascular morphogenesis in the mouse retina. *Dev Cell* **57**, 2321-2333 e2329, doi:10.1016/j.devcel.2022.09.002 (2022).
53 Gerber, H. P. *et al.* VEGF is required for growth and survival in neonatal mice. *Development* **126**, 1149-1159, doi:10.1242/dev.126.6.1149 (1999).
54 Hayashi, S. & McMahon, A. P. Efficient recombination in diverse tissues by a tamoxifen-inducible form of Cre: a tool for temporally regulated gene activation/inactivation in the mouse. *Dev Biol* **244**, 305-318, doi:10.1006/dbio.2002.0597 (2002).
55 Zheng, G. X. *et al.* Massively parallel digital transcriptional profiling of single cells. *Nat Commun* **8**, 14049, doi:10.1038/ncomms14049 (2017).
56 Hao, Y. *et al.* Dictionary learning for integrative, multimodal and scalable single-cell analysis. *Nat Biotechnol* **42**, 293-304, doi:10.1038/s41587-023-01767-y (2024).
57 Hafemeister, C. & Satija, R. Normalization and variance stabilization of single-cell RNA-seq data using regularized negative binomial regression. *Genome Biol* **20**, 296, doi:10.1186/s13059-019-1874-1 (2019).
58 Ji, Z. & Ji, H. TSCAN: Pseudo-time reconstruction and evaluation in single-cell RNA-seq analysis. *Nucleic Acids Res* **44**, e117, doi:10.1093/nar/gkw430 (2016).
59 La Manno, G. *et al.* RNA velocity of single cells. *Nature* **560**, 494-498, doi:10.1038/s41586-018-0414-6 (2018).
60 Atta, L., Sahoo, A. & Fan, J. VeloViz: RNA velocity-informed embeddings for visualizing cellular trajectories. *Bioinformatics* **38**, 391-396, doi:10.1093/bioinformatics/btab653 (2022).
61 Zarkada, G. *et al.* Specialized endothelial tip cells guide neuroretina vascularization and blood-retina-barrier formation. *Dev Cell* **56**, 2237-2251 e2236, doi:10.1016/j.devcel.2021.06.021 (2021).
62 Sanjana, N. E., Shalem, O. & Zhang, F. Improved vectors and genome-wide libraries for CRISPR screening. *Nat Methods* **11**, 783-784, doi:10.1038/nmeth.3047 (2014).
63 Jostes, S. V. *et al.* Unique and redundant roles of SOX2 and SOX17 in regulating the germ cell tumor fate. *Int J Cancer* **146**, 1592-1605, doi:10.1002/ijc.32714 (2020).

Figure 1: Blocking VEGFR2 signaling increases arterial specification.
a-d. Mouse neonatal retinas dissected at p6, followed by immunostaining of Isolectin B4 (IB4) and antibodies targeting smooth muscle actin (SMA) and Sox17. Yellow dashed lines indicate the vascular frontline. White dashed brackets indicate the gap distance between Sox17-labeled arterial tip to the vascular front. **a**. Control and *Vegfa*^{iKO} retinas dissected at p6 (tamoxifen induction of gene deletion at p2, 4). **b**. Control and *Vegfr2*^{iECKO} retinas dissected at p6 (tamoxifen-induced gene deletion at p2-4). **c**. Control and *Plcg1*^{iECKO} retinas (tamoxifen induction of gene deletion at p1-3). **d.** Retinas from pups treated with two doses of IgG or DC101 antibody injection at p1 (400μg) and p3(200μg). Blue dashed rectangles in the quantification plots per artery indicate the arteries with full extension and no un-arterialized gap from the artery tip to the vascular front. Abbreviations: A: artery; V: vein. Scale bars: 500 μm (the left columns in a-d); 100μm (the right 3 columns in a-d). Two tailed, unpaired Student t-test was used for statistics. A p value equal to or less than 0.05 was determined as statistically significant, in extents demonstrated by asterisks * ($p \leqslant 0.05$), ** ($p \leqslant 0.01$), *** ($p \leqslant 0.001$), **** ($p \leqslant 0.0001$). Numeric values are reported for p values greater than 0.05.

Figure 2: Fluid shear stress-induced arterial program is independent of VEGFR2 signaling.
a. Mouse postnatal retinas were dissected at p6. Before dissection, IB4 (green) was retro-orbitally injected to perfuse the retina vasculatures of Control, DC101-treated, *Vegfr2*^{iECKO} and *Plcg1*^{iECKO} mice. Dissected retinas were stained with IB4 (red) to visualize all perfused and non-perfused blood vessels. Perfused vessels are double-stained (IB4-green/red), while vessels not perfused were single-stained (IB4-red only, indicated by white arrow heads). Abbreviations: A: artery; V: vein. Scale bars: 100μm. **b**. HUVECs with siPLCg1 treatments were subjected to static (ST) or FSS (12dyn/cm^2) for 16 hours to induce arterial differentiation. Gene expression was examined by quantitative RT-PCR followed by quantification relative to ST-siCTRL. Two-way ANOVA with multiple comparisons was used for statistics. A p value equal to or less than 0.05 was determined as statistically significant, in extents demonstrated by asterisks * ($p \leqslant 0.05$), ** ($p \leqslant 0.01$). ns: not significant. Error bars indicate standard error of the mean.

Fig.3 Blocking VEGFR2 signaling promotes capillary-to-artery transition.
a. Arteriovenous zonation in combined control and *Plcg1*^{iECKO} retinal ECs. **b**. Distributions of control and *Plcg1*^{iECKO} retinal ECs in clusters 0-9. Quantification plots demonstrating percentage and log2 fold change of the cells in clusters 0-9 in control and *Plcg1*^{iECKO}. **c**. Pseudotime trajectory analysis by TSCAN. **d.** RNA velocity analysis demonstrating transitioning trajectories of control and *Plcg1*^{iECKO} retinal ECs.

Figure 4. VEGF-A counteracts FSS-driven capillary-to-artery cell fate transition.
a-e. HMVBECs were cultured in the conditions of static (ST), VEGF (20ng/ml), FSS (12dyn/cm^2) and FSS+VEGF for 16 hours. Gene expression was examined by bulk RNAseq, validated by quantitative RT-PCR and western blot. **a.** Principal component analysis (PCA) of RNAseq data. **b.** cSTAR analysis of RNAseq data. DPD scores of EC states shown in 3D space of the STV_{FSS}, STV_{VEGF}, and STV_{SSVA}. Four EC states correspond to different FSS and VEGF treatments. A change in the EC phenotype is quantified by the DPD score along the corresponding STV. The first cSTAR step uses a machine learning technique called support vector machines (SVM) to exploit the high-dimensional transcriptomics space and construct separating surfaces between distinct EC states. Subsequently, the directions of EC state conversions are determined in the transcriptomic space. These directions are the shortest paths from one EC state to another state, which are specified by the State Transition Vectors

(STVs). STVs are unit vectors defined as normal vectors to the hyperplanes that separate EC phenotypic states. After building the STVs, cSTAR calculates quantitative indicators of cell phenotypic states termed Dynamic Phenotype Descriptors (DPD). For EC cells in different states, the DPD scores describe phenotypic features associated with each STV[28,29]. The STV_{FSS} indicates the shortest path from an EC ST state to a FSS state, and the DPD_{FSS} quantifies a normalized FSS-related score of the changes in the transcriptomics patterns. The STV_{VEGF} indicates the direction from an ST state to a new EC state caused by VEGF stimulation at zero FSS, whereas the DPD_{VEGF} scores quantify the extent of the transcriptomics changes related to VEGF stimulation. The angle between two directions of the transcriptomics changes, STV_{FSS} and STV_{VEGF} is 84 degrees. The near orthogonality of these two STVs suggests mutually independent transcriptomic changes between the FSS and VEGF EC states, with any slight deviation from orthogonality indicating a minor overlap in the regulatory pathways induced by FSS or VEGF. To better understand changes in the transcriptomic profile of the FSS EC state brought about by VEGF stimulation, we built the STV_{SSVA} to determine the direction of the EC FSS state change induced by a combined FSS and VEGF stimulation. The resulting STV_{SSVA} appears to be almost orthogonal to both STVs determined above (the angle between the two vectors, STV_{SSVA} and STV_{FSS} is 89 degrees, and the angle between the STV_{SSVA} and the STV_{VEGF} is 87 degrees suggesting that this combination (VEGF+FSS) leads to a new state distinct from both STV_{VEGF} and $STV_{FSS.}$ Based on the STV_{SSVA}, we next calculated the DPD_{SSVA} that scores the changes in the phenotypic cell features following combined FSS and VEGF treatment. A combined VEGF and FSS treatment only slightly increases the DPD_{VEGF} score of the FSS state and does not change the DPD_{FSS} score. **c.** Transcriptomic differential gene expression analysis clusters the arterial and capillary genes regulated by ST, ST+VEGF, FSS and FSS+VEGF. **d-e.** Expression of arterial and capillary genes assayed by quantitative RT-PCR (**d**) and western blot (**e**). **f**. Reciprocal expression pattern of arterial and capillary markers. Immunostaining of arterial markers Sox17 or SMA, co-stained with capillary genes Mfsd2a, Emcn, Flt4 and TFR, respectively, in P5 mouse neonatal retina. **g.** Western blot results of HMVBECs cultured in the conditions of ST, FSS with a gradient of VEGF (0, 2, 10, 20ng/ml). **h.** Western blot of siRNA-treated HUVECs subjected to ST, FSS and FSS+VEGF. **i**. A working model demonstrating opposite roles of VEGF and FSS on capillary-to-artery cell fate transition. One-way ANOVA with multiple comparisons was used for statistics. A p value equal to or less than 0.05 was determined as statistically significant, in extents demonstrated by asterisks * ($p \leqslant 0.05$), ** ($p \leqslant 0.01$), *** ($p \leqslant 0.001$), **** ($p \leqslant 0.0001$). ns: not significant.

Figure 5. VEGF-A does not use Notch to counteract the FSS-arterial program.
Pretreated with DMSO or 5uM DAPT for 3h, HMVBECs were harvested (FSS 0 hr) or subjected to FSS with DMSO or DAPT for 16 hr. Samples were analyzed by western blot. One-way ANOVA with multiple comparisons was used for statistics. A p value equal to or less than 0.05 was determined as statistically significant, in extents demonstrated by asterisks * ($p \leqslant 0.05$), ** ($p \leqslant 0.01$). ns: not significant.

Figure 6. Sox17 mediates FSS-induced arterial fate specification.
a. HUVECs lentivirally transduced with CRISPR-Cas9-directed sgNT, sgSox17, sgSox18 or combined sgSox17/18 were used to test FSS-induced arterial differentiation. Cell lysates were analyzed by western blot. **b.** HUVECs harboring a doxycycline-inducible Sox17 expression system (pCW57.1-hSox17-myc-DDK) were treated by a gradient of doxycycline (DOX) for 48 hours. Cell lysates were analyzed by western blot. One-way ANOVA with multiple comparisons was used for statistics. A p value equal to or less than 0.05 was determined as statistically significant, in extents demonstrated by asterisks * ($p \leqslant 0.05$), ** ($p \leqslant 0.01$), *** ($p \leqslant 0.001$), **** ($p \leqslant 0.0001$). ns: not significant.

Figure 7 VEGF-A antagonizes Sox17-mediated transcription regulation of the arterial program..
a-c. HUVECs harboring a doxycycline-inducible Sox17 expression system (pCW57.1-hSox17-myc-DDK) were used for these experiments for 48 hours. **a.** Quantitative RT-PCR analysis of RNA expression under experimental conditions of no treatment (NT), DOX (1000ng/ml) and DOX (1000ng/ml)+VEGF (50ng/ml). Definitive arterial genes (Gja5, Gja4, Sema3g, Jag1, Cxcl12 and Efnb2) and VEGF-Notch (V-N) targets (Unc5b and Dll4) were tested. **b.** A dose gradient of VEGF (0-100ng/ml) was used to test the impact on DOX-induced arterial differentiation. Cell lysates were analyzed by western blot. **c.** Chromatin immunoprecipitation (ChIP) results of Sox17 enrichment on the promoters and enhancers of the definitive arterial genes. The results are demonstrated by fold changes of percentage input relative to NT. **d.** Working model: VEGF signaling counteracts FSS-induced arterial specification by compromising Sox17-mediated transcription regulation. Gja4 is used as an example in this diagram. Left: in the absence of VEGF signaling, FSS-induced Sox17 is enriched at its binding motifs on arterial promoters and enhancers, forming an activating transcription complex to turn on arterial gene expression. Right: VEGF signaling compromises the enrichment of Sox17 on arterial promoters and enhancers, thereby turning off the expression of arterial gene. One-way ANOVA with multiple comparisons was used for statistics. A p value equal to or less than 0.05 was determined as statistically significant, in extents demonstrated by asterisks * ($p \leqslant 0.05$), ** ($p \leqslant 0.01$), *** ($p \leqslant 0.001$), **** ($p \leqslant 0.0001$). ns: not significant.

Figure 8. VEGF-FSS crosstalk controls the extent of arteriogenesis, angiogenesis and capillary maintenance. **a.** Trajectories of vascular morphogenesis in mouse neonatal retina. The developing vasculature originates from the vein that gives rise to the capillary bed. Sprouting angiogenesis expands the capillary bed towards the peripheral avascular zone. At the same time, the capillary bed undergoes a remodeling process to form arteries. **b.** VEGF is a physiological brake that antagonizes FSS-induced arterialization in the capillary bed. A hypothetical model of vascular morphogenesis under physiological condition or blocked VEGFR2 signaling. Red arrows indicate the directionality of arterial (dark red) and post-arterial (light red) FSS, respectively. Blue arrows indicate the directionality of pre-venous (light blue) and venous (dark blue) FSS, respectively. The shaded artery-associated capillary area between the arterial tip and the vascular front is defined as the “Arterial Delta” in this study. Exposed to effective post-arterial FSS from the artery and VEGF diffused from the juxtaposed avascular zone, Arterial Delta is where VEGF-FSS competition on arterial specification takes place. Blocking VEGFR2 signaling removes the physiological brake that counteracts the FSS-induced arterial program, leaving FSS as the sole player that ectopically arterialize the Arterial Delta capillary and beyond. **c.** VEGF and FSS counteract to control angiogenesis and arteriogenesis from the capillary bed. The condition with high level of VEGF and low FSS favors angiogenesis and inhibits arteriogenesis, while arteriogenesis requires a decline of VEGF signaling as a permissive prerequisite to allow high arterial level of FSS to drive arterial specification.

Supplemental figure 1. Arteriogenesis occurs in the capillary regions of low VEGF signaling.
a. Formation and remodeling of the capillary bed in mouse postnatal retina. Mouse retinas were dissected at P1-4, followed by immunostaining of Sox17 and IB4. The arrow in P2 indicates emergence of arterial morphogenesis labeled by high level of Sox17 expression. **b.** Left column: p5 retina was immunostained with EdU, Erg and IB4. Middle and right columns: immunostaining of pERK and IB4 on P5 retina. i.v.: intravenous (retro-orbital) injection. Abbreviations: A: artery; V: vein. Scale bars: 100μm.

Supplemental figure 2. Deletion of endothelial VEGFR2 in postnatal mouse retina.
a. IB4 immunostaining of control and VEGFR2^{iECKO} retinas at P5. Tamoxifen was injected at P0-2. **b.** Control and *VEGFR2^{iECKO}* retinas dissected at p5 (tamoxifen-induced gene deletion at p1-3). Retinas were immunostained by Sox17, SMA and IB4. Pink arrow heads indicate ectopic arterialization at the vascular front. Question marks labeled the vessels with ambiguous arteriovenous patterning, likely arterialized veins. Blue arrow heads indicate minor arteriogenesis. **c.** Control and *VEGFR2^{iECKO}* retinas immunostained with IB4 and VEGFR2 to visualize endothelial-specific deletion of VEGFR2. The areas in the white dashed squares are shown in higher magnification in the images of the next column. White arrow heads indicate Sox17^{high}/VEGFR2^{+} ECs in the control mice. Blue arrow heads indicate Sox17^{high}/VEGFR2^{null} ECs. Abbreviations: A: artery; V: vein. Scale bars: 300μm(a), 100μm (b and c).

Supplemental figure 3. Endothelial deletion of PLCγ1 during postnatal development.
a. A demonstration of the exons in mouse PLCg1 gene in control and *Plcg1^{iECKO}*. Two loxP sites flank exons 2-4, which are excised in *Plcg1^{iECKO}*. Two sets of PCR primers were designed to detect Exons2-3 (Ex2-3) or downstream Exons 24-26 (Ex24-26). **b.** Brains from control and *PLCγ1^{iECKO}* pups at P6 (tamoxifen induction at P1-3) were first enriched by magnetic activated cell sorting (MACS) and further sorted by Fluorescence-activated cell sorting (FACS) in flow cytometry sorting out the CD31+ (APC)/CD45- (BV421)/PI- (PE) ECs. Plcg1 mRNA was detected by primer sets for Ex2-3 or Ex24-26. **c.** Distribution of retinal ECs with Plcg1 RNA expression in GEM-X 3' scRNAseq.

Supplemental figure 4. Arterial Notch activity is independent of VEGFR2 signaling.
Control, *PLCγ1^{iECKO}* and *VEGFR2^{iECKO}* retinas with a background of Notch reporter CBF:H2B-Venus were immunostained with Sox17 and IB4. Nuclear CBF signal was natural venus fluorescence.The areas in the white dashed squares are shown in higher magnification in the images of the bottom two rows. White arrow heads indicate arterial ECs colocalized with CBF-Venus signal.

Supplemental figure 5. Clustering of endothelial cells in a single-cell transcriptome.
30 clusters of cells from control and *Plcg1^{iECKO}* retinas were identified and demonstrated in UMAP. Endothelial cells in cluster 12 were identified by high expression levels of Pecam1, Cdh5 and Cldn5.

Supplemental figure 6. Mapping arteriovenous zonation in a single cell transcriptome.
a. Identification of clusters 0-9 in all combined control and *Plcg1^{iECKO}* endothelial cells. **b.** Cluster 6 enriched with Esm1 and Kcne3 is identified as sprouting ECs. **c-d.** The cells in Cluster 9 expressing high level of arterial markers are arterial ECs. Clusters 0, 2, 3, 4, 6, 7 are identified as capillary/venous clusters. The cells in Cluster 8 are arterial predecessors with both arterial and capillary profiles. The ECs in Cluster 1 have weak capillary identity. **e.** The ECs in Cluster5 express low levels of endothelial markers, likely losing endothelial identity. **f.** Mapping cell cycle. Cluster 0 identified as proliferative capillary ECs mostly in G2/M phase.

Supplemental figure 7. VEGF-FSS crosstalk regulates arterial specification in HUVECs.
HUVECs were subjected to the conditions of static (VEGF-/FSS-), ST with 20ng/ml VEGF (VEGF+/FSS-), 12dyn/cm^2 FSS (FSS+/VEGF-) and FSS+VEGF (FSS+/VEGF+). Gene expression was examined by western blot. While most definitive arterial genes responded to VEGF and VEGF+FSS the same manner as HMVBECs (Fig.4), FSS induction of Sox17 and Nrp1 in HUVECs is further promoted by VEGF. One-way ANOVA with multiple comparisons was used for statistics. A p value equal to or

less than 0.05 was determined as statistically significant, in extents demonstrated by asterisks * ($p \leqslant 0.05$), ** ($p \leqslant 0.01$). ns: not significant.

Supplemental figure 8. Arterial specification requires Notch signaling.
a. P5 retina of Notch reporter line CBF:H2B-Venus. Arterial ECs were labeled by immunostaining of Sox17. Notch activity was visualized by endogenous Venus (CBF) signal in the nuclei. Arrow heads indicate Sox17^{high}/CBF- arterial ECs. Scale bars: 25 μm. **b.** A 20-hour time course of FSS-induced Notch signaling and expression of arterial genes in HMVBECs. **c.** P5 retinas from Ctrl and *Dll4*^{iECKO} pups, treated with IgG or DC101 injection at p1 and p3. IB4 (green) was retro-orbitally injected to perfuse the lumenized blood vessels. Dissected retinas were immunostained with Sox17 and IB4 (blue). Abbreviations: A: artery; V: vein. Scale bars: 10μm (a), 100 μm (c).

Supplemental Table 1. Endothelial markers for mapping arteriovenous zonation.

Supplemental Table 2. A matrix of the DPD scores.

Supplemental Table3. Predicted transcription factor binding motifs of Sox17 and RBPJ in arterial and capillary genes (TRANSFACT).

Supplemental Table 4. Genotyping primers

Supplemental Table 5. Antibodies for immunostaining.

Supplemental Table 6. siRNA information.

Supplemental Table 7. QPCR primers

Supplemental Table 8. Antibodies for western blot.

Supplemental Table 9. QPCR primers for ChIP.

Fig.1 Blocking VEGFR2 signaling increases arterial specification.

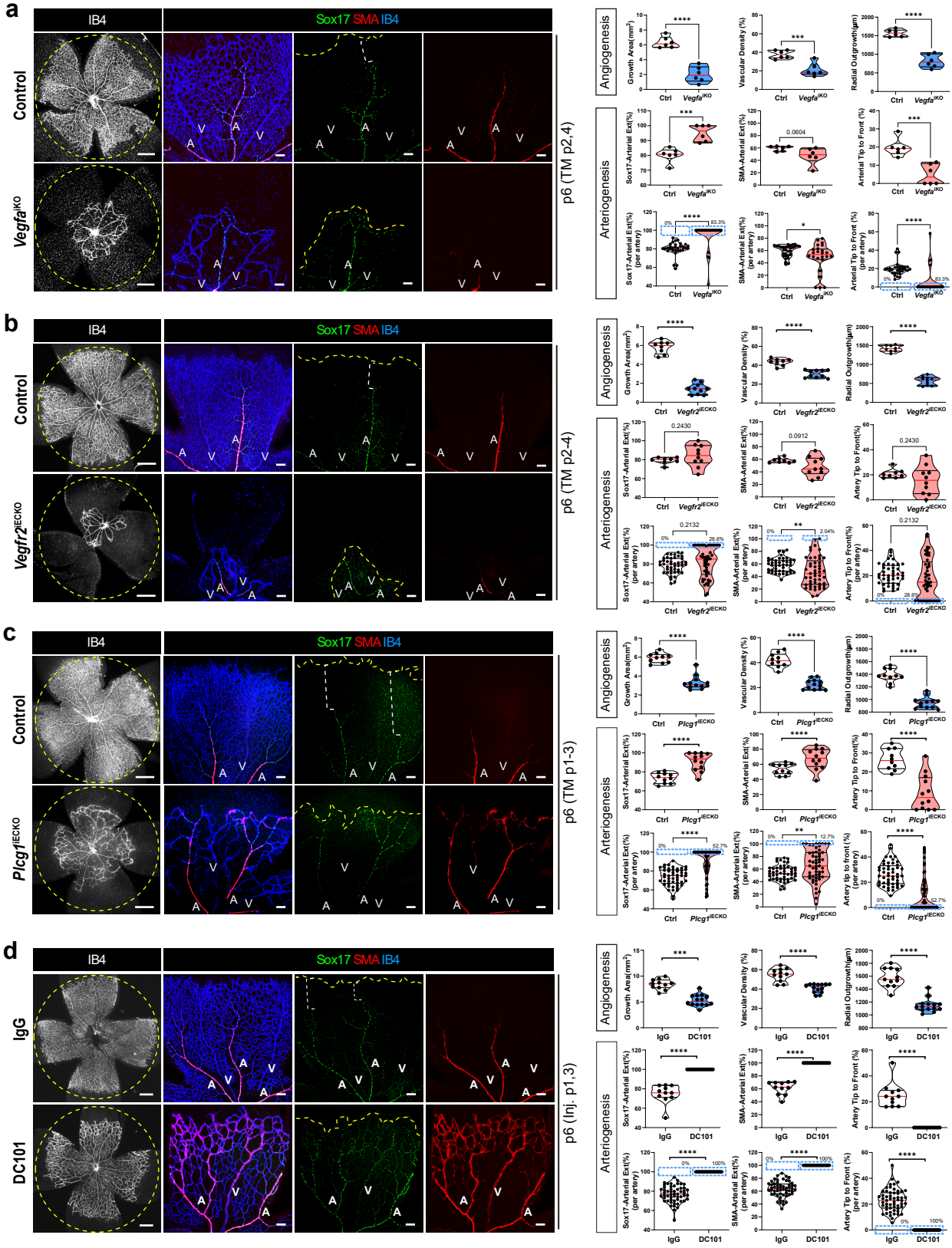

Fig.2 Fluid shear stress-induced arterial program is independent of VEGFR2 signaling.

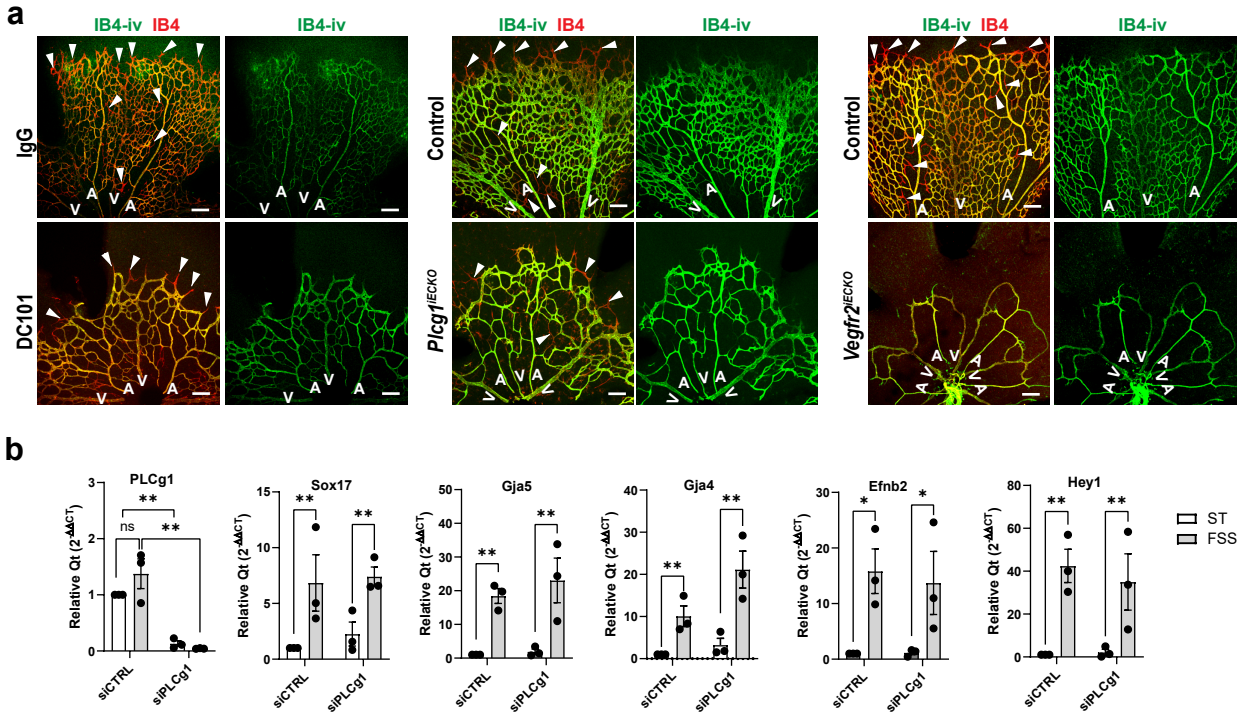

Fig.3 Blocking VEGFR2 signaling promotes capillary-to-artery transition.

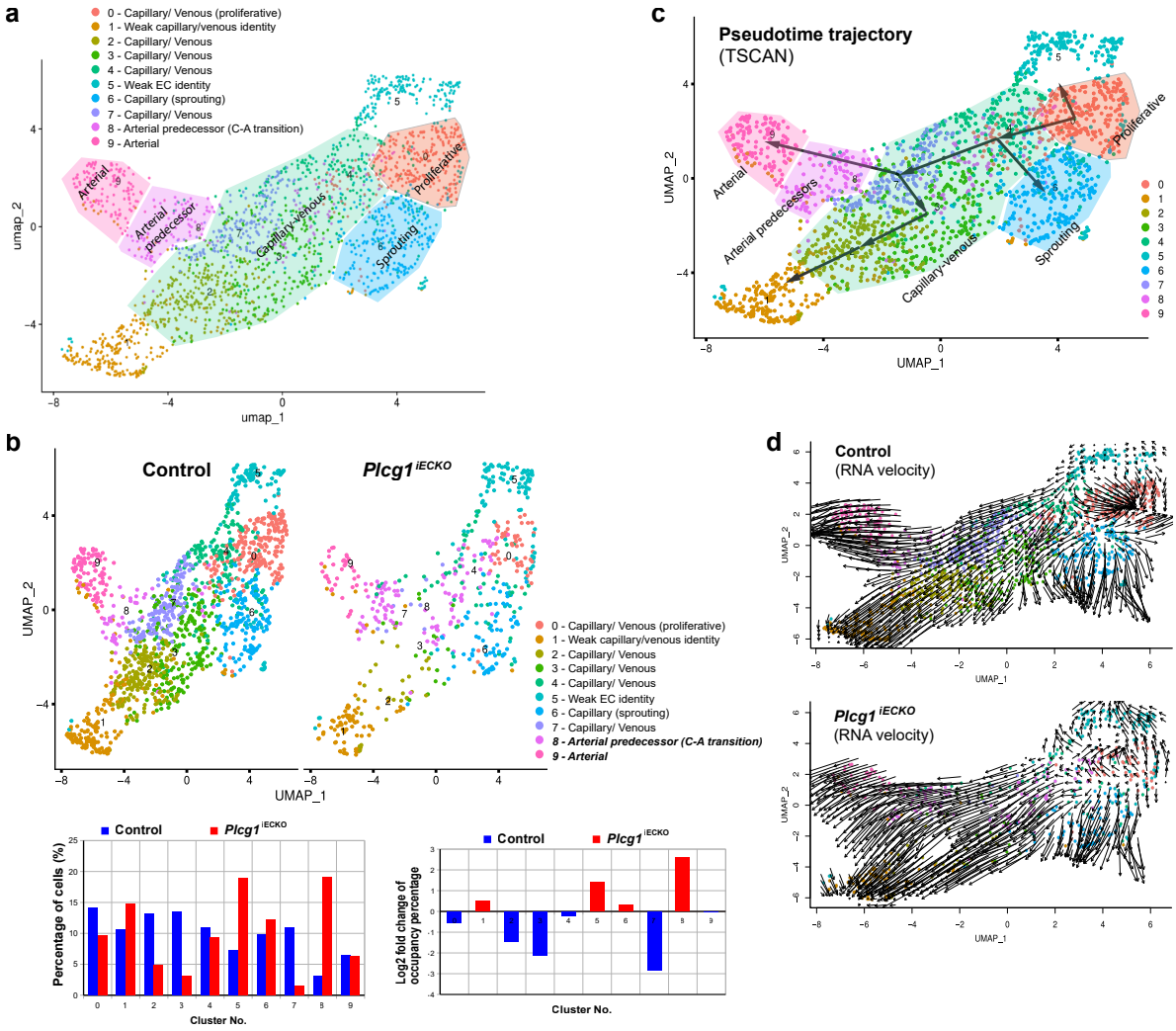

Fig.4 VEGF-A counteracts FSS-driven capillary-to-artery cell fate transition.

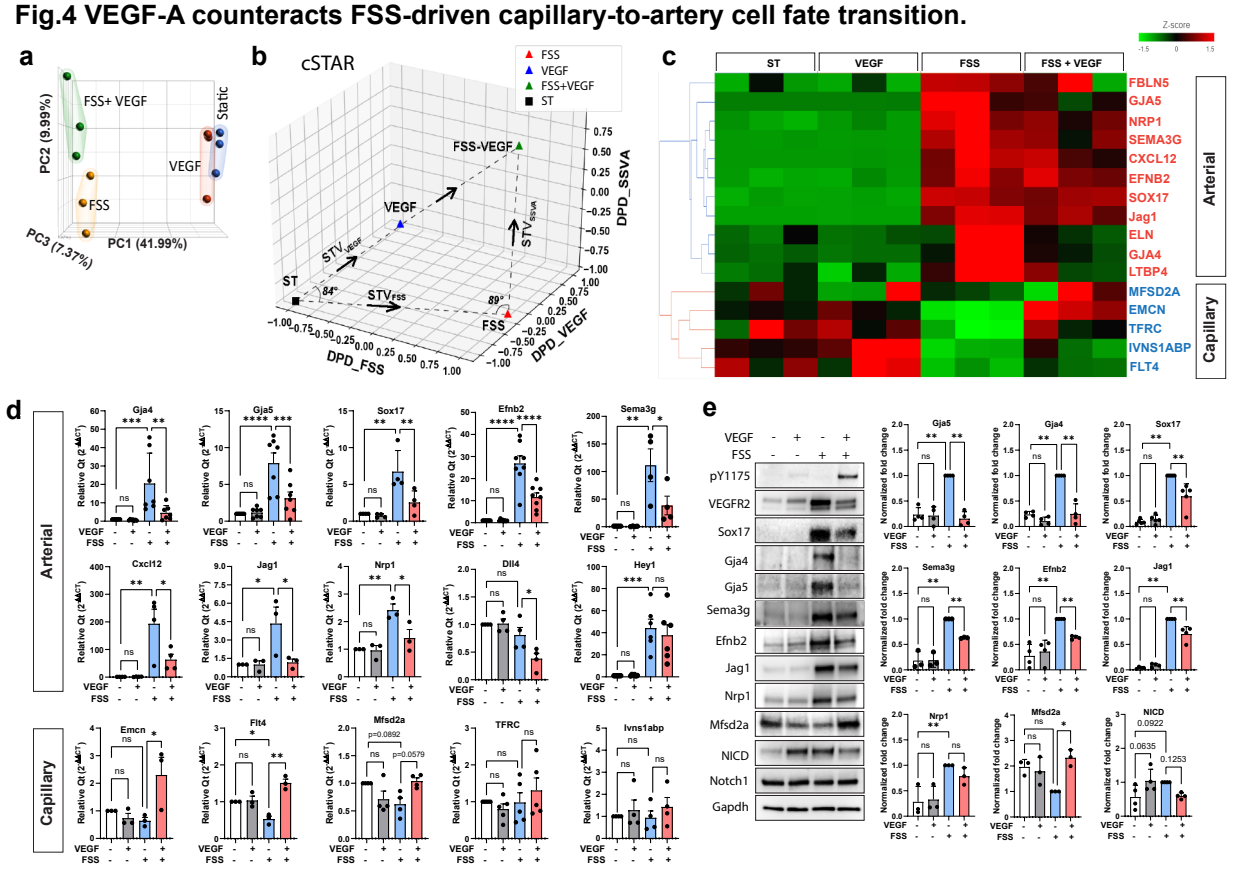

Fig.5 VEGF-A does not use Notch to counteract the FSS-arterial program.

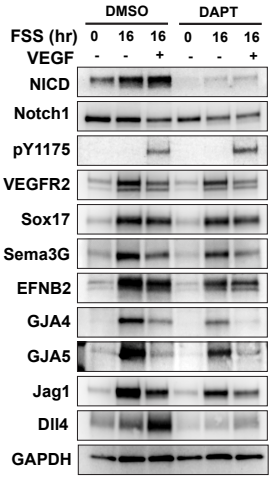

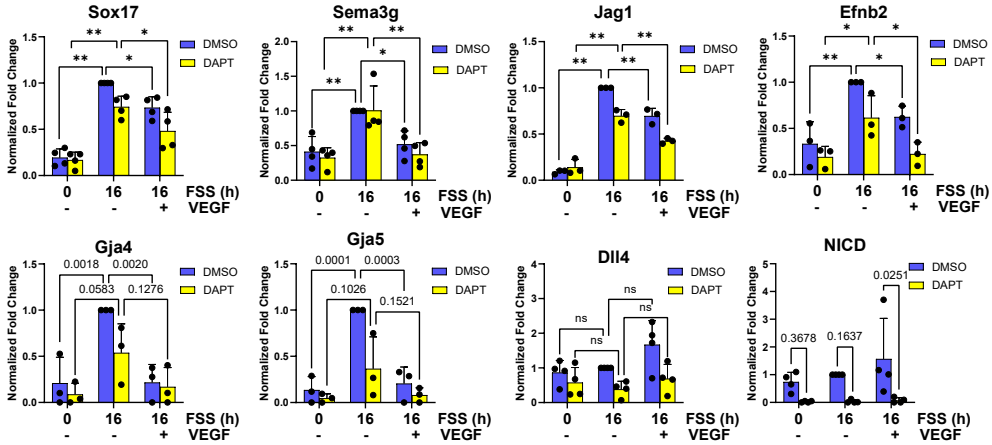

Fig.6 Sox17 mediates FSS-induced arterial fate specification.

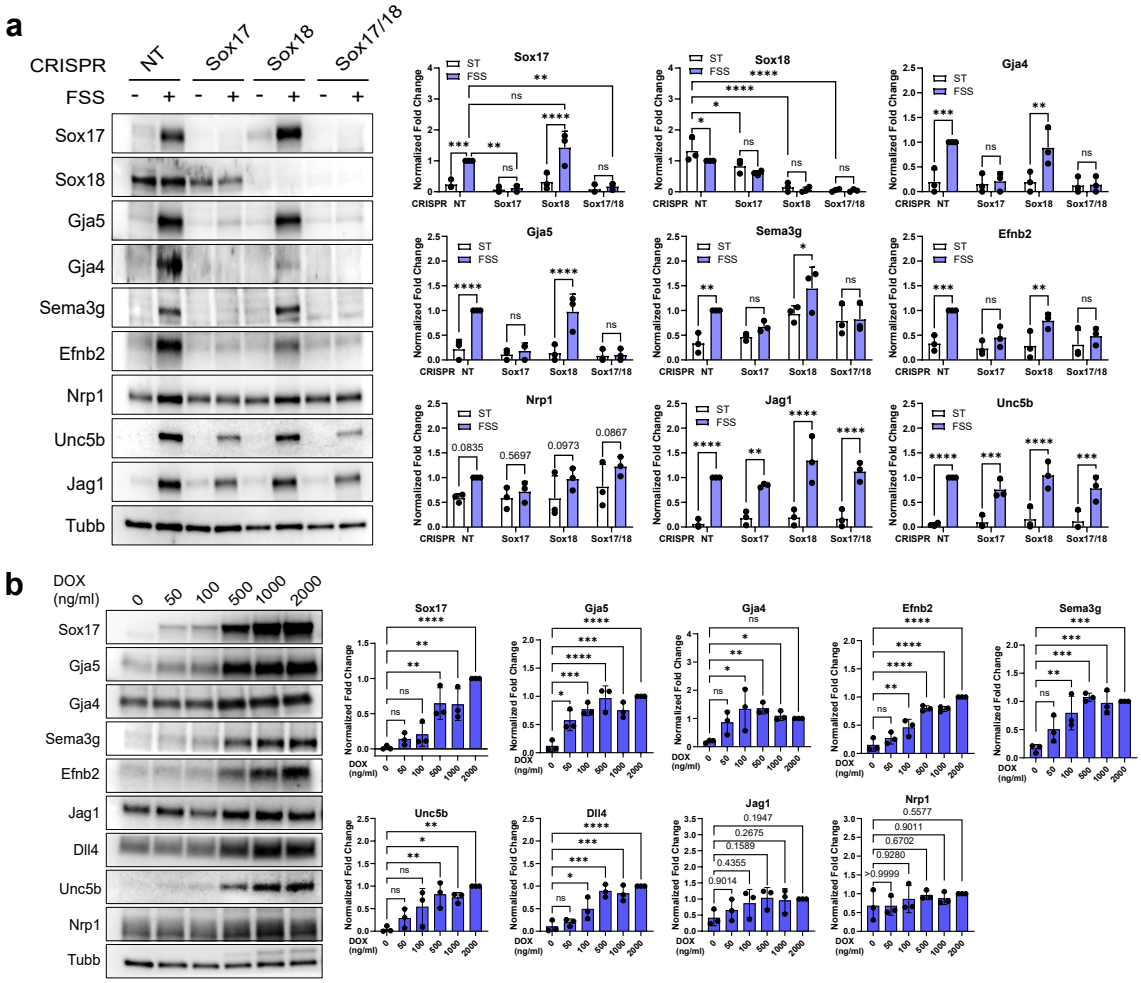

Fig. 7 VEGF-A anatagonizes Sox17-mediated transcription regulation of the arterial program.

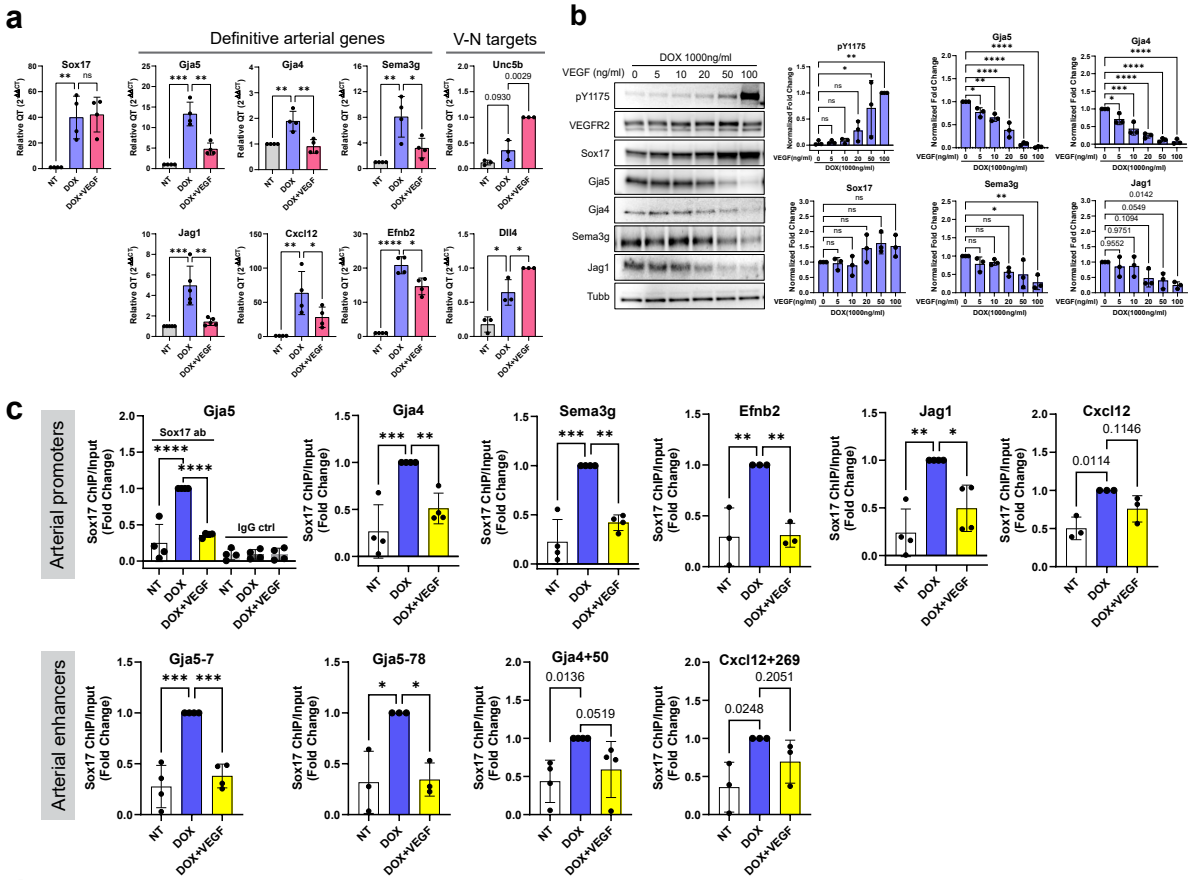

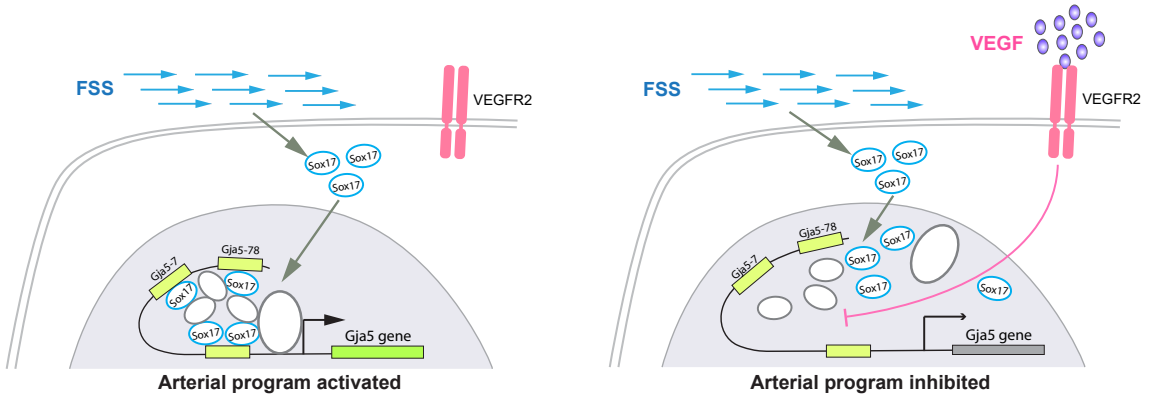
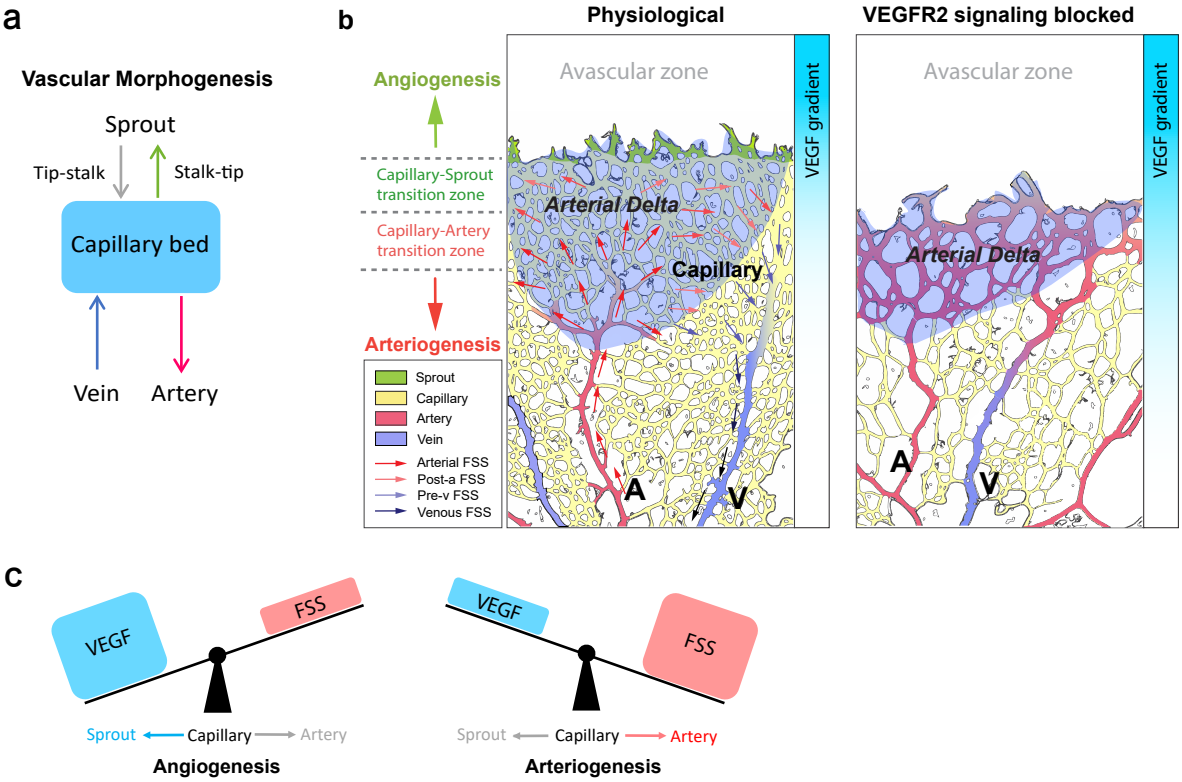
Fig.8 VEGF-FSS crosstalk controls the extent of arteriogenesis, angiogenesis and capillary maintenance.